

A NUMERICAL STUDY OF CONJUGATE FLOWS AND
FLAT-CENTRED INTERNAL SOLITARY WAVES IN A
CONTINUOUSLY STRATIFIED FLUID

CENTRE FOR NEWFOUNDLAND STUDIES

**TOTAL OF 10 PAGES ONLY
MAY BE XEROXED**

(Without Author's Permission)

BANGJUN WAN



INFORMATION TO USERS

This manuscript has been reproduced from the microfilm master. UMI films the text directly from the original or copy submitted. Thus, some thesis and dissertation copies are in typewriter face, while others may be from any type of computer printer.

The quality of this reproduction is dependent upon the quality of the copy submitted. Broken or indistinct print, colored or poor quality illustrations and photographs, print bleedthrough, substandard margins, and improper alignment can adversely affect reproduction.

In the unlikely event that the author did not send UMI a complete manuscript and there are missing pages, these will be noted. Also, if unauthorized copyright material had to be removed, a note will indicate the deletion.

Oversize materials (e.g., maps, drawings, charts) are reproduced by sectioning the original, beginning at the upper left-hand corner and continuing from left to right in equal sections with small overlaps. Each original is also photographed in one exposure and is included in reduced form at the back of the book.

Photographs included in the original manuscript have been reproduced xerographically in this copy. Higher quality 6" x 9" black and white photographic prints are available for any photographs or illustrations appearing in this copy for an additional charge. Contact UMI directly to order.

UMI

A Bell & Howell Information Company
300 North Zeeb Road, Ann Arbor, MI 48106-1346 USA
313/761-4700 800/521-0600

**A NUMERICAL STUDY OF CONJUGATE FLOWS
AND FLAT-CENTRED INTERNAL SOLITARY
WAVES IN A CONTINUOUSLY STRATIFIED FLUID**

By

©Bangjun Wan, B.Eng., M.Sc.

**A thesis submitted to the School of Graduate
Studies in partial fulfillment of the
requirements for the degree of
Master of Science**

**Department of Physics and Physical Oceanography
Memorial University of Newfoundland**

July, 1997

St. John's

Newfoundland

Canada



National Library
of Canada

Acquisitions and
Bibliographic Services

395 Wellington Street
Ottawa ON K1A 0N4
Canada

Bibliothèque nationale
du Canada

Acquisitions et
services bibliographiques

395, rue Wellington
Ottawa ON K1A 0N4
Canada

Your file *Votre référence*

Our file *Notre référence*

The author has granted a non-exclusive licence allowing the National Library of Canada to reproduce, loan, distribute or sell copies of this thesis in microform, paper or electronic formats.

The author retains ownership of the copyright in this thesis. Neither the thesis nor substantial extracts from it may be printed or otherwise reproduced without the author's permission.

L'auteur a accordé une licence non exclusive permettant à la Bibliothèque nationale du Canada de reproduire, prêter, distribuer ou vendre des copies de cette thèse sous la forme de microfiche/film, de reproduction sur papier ou sur format électronique.

L'auteur conserve la propriété du droit d'auteur qui protège cette thèse. Ni la thèse ni des extraits substantiels de celle-ci ne doivent être imprimés ou autrement reproduits sans son autorisation.

0-612-25896-3

Canada

Abstract

In this thesis a theoretical model describing the limiting flow structure in the centre of a fully nonlinear, flat-centred internal solitary wave in a fluid of finite depth H has been developed using the conjugate flow concept. The conjugate flow solution gives the vertical structure of the isopycnal displacement and the fluid velocity at the centre of a flat-centred internal solitary wave as well as the propagation speed of the wave. The mode-1 internal solitary waves are calculated in a continuously stratified fluid given by hyperbolic tangent density profiles with one or two pycnoclines. Solutions obtained with and without the Boussinesq approximation are compared. The non-Boussinesq results are almost identical with the Boussinesq results if the surface to bottom density difference is 4% or less unless the pycnoclines have a thickness comparable to the total fluid depth.

For density stratifications with a single pycnocline, conjugate flow solutions are obtained when the pycnocline is not too close to the boundary. The size of the valid solution range decreases as the thickness of pycnocline increases. When the Boussinesq approximation is applied, the magnitude of the extreme isopycnal displacement grows as the centre of the pycnocline in the undisturbed region moves away from the mid-depth: the wave propagation speed increases as the centre of pycnocline moves toward the mid-depth. If the thickness of the pycnocline is greater than 8.4% of the fluid depth, the parallel shear flow in the centre of a flat-centred internal solitary wave is linearly stable. As the pycnocline gets narrower the flow becomes potentially

unstable over an increasing range of pycnocline heights.

For stratifications with two pycnoclines multiple conjugate flow solutions may exist. When the two pycnoclines are equidistant from the mid-depth, one above and one below, there are two solutions if the pycnoclines are well separated and not too close to the boundaries. If the pycnoclines are close together there are no solutions if the Boussinesq approximation is made and one solution if the approximation is not made. If the two pycnoclines are not equidistant from the mid-depth there can be 0, 1, 2, or 3 solutions. Flat-centred wave can exist only if there is a conjugate flow solution, but the converse is not true. Having a conjugate flow solution does not necessarily mean that there is a flat-centred internal solitary wave.

Acknowledgements

I would like to express my sincerest thanks to Dr. Kevin G. Lamb, my supervisor, who outlined the research idea of this thesis work and offered continual guidance and comments during the completion of my thesis. He reviewed the manuscript with great patience and gave invaluable suggestions and comments which made a great contribution to the completion of this thesis. Dr. Lamb also kindly provided me with financial support throughout the course of this work.

I am also indebted to Dr. Richard Greatbatch for his academic assistance and encouragement during my studies.

I am grateful to Mr. Allan Goulding, Mr. Kenneth Forward, Dr. Andrew Peterson and Mr. Helmut Roth for their help in solving my computer problems. Thanks are also given to Guoqing Li and Fraser Davidson for their help.

I would also like to express my gratitude to my mother and my wife for their unwavering support and encouragement.

This work was partially supported by the School of Graduate Studies and Department of Physics and Physical Oceanography of Memorial University of Newfoundland through Graduate Fellowships and Graduate Assistantships.

Contents

1	Introduction	1
2	Conjugate Flow Model	11
3	Computational Model for Fully Nonlinear Internal Solitary Waves	24
3.1	Governing Equations	24
3.2	Numerical Method	33
4	Verification that the Flow in the Centre of a Flat-Centred Internal Solitary Wave is Given by the Conjugate Flow Solutions	39
4.1	Model Initialization	40
4.2	Model Results	43
5	Results for Single Pycnocline Density Stratifications	53
5.1	Results for the First Density Stratification	55
5.2	Results for the Second Density Profile	72

6	Results for Density Stratifications with Two Pycnoclines	78
6.1	Case 1: $a_1 = a_2 = a$, $d_1 = d_2 = d$, $z_2 = H - z_1$	79
6.2	Case 2: $a_1 = a_2 = a$, $d_1 = d_2 = d$, $z_2 \neq H - z_1$	82
6.3	Case 3: $a_1 \neq a_2$, $d_1 = d_2 = d$	91
6.4	Case 4: $a_1 = a_2 = 0.01$, $d_1 \neq d_2$, $z_1 \neq H - z_2$	95
6.5	Internal Solitary Waves Corresponding to Conjugate Flow Solutions .	96
7	Summary and Conclusion	102

List of Figures

2.1	Geometrical interpretation of isopycnals passing through point (x, z) and $(x, z + dz)$ in the conjugate flow region.	14
3.1	Geometrical interpretation of the vertical displacement $\eta(x, z)$ of an isopycnal surface passing through a point (x, z)	27
4.1	Density profile for density 1 with $a = 0.01$, $z_0 = 70$ and $d = 10$	41
4.2	Buoyancy frequency profile for density 1 with $a = 0.01$, $z_0 = 70$ and $d = 10$	41
4.3	Surface current profiles for different A values. Density 1 with $a = 0.01$, $z_0 = 70$ and $d = 10$. $A = 0.1, 0.25, 0.5, 1, 2, 3, 4, 5, 7, 10, 15, 20, 25, 30, 50, 70, 100, 120$	45

4.4	Magnitude of the extreme isopycnal displacement η_{ext} as a function of A for density 1 with $a = 0.01$, $z_0 = 70$ and $d = 10$. Solid line: fully nonlinear model results; dashed line: magnitude of the extreme isopycnal displacement calculated from the conjugate flow model. Stars correspond to the values of A used.	45
4.5	Variation of wave half-length λ with A for density 1 with $a = 0.01$, $z_0 = 70$ and $d = 10$	46
4.6	Wave propagation speed c plotted as a function of A for density 1 with $a = 0.01$, $z_0 = 70$ and $d = 10$. Solid line: fully nonlinear model results, dashed line: conjugate flow model results. Stars correspond to the values of A used.	46
4.7	Wave half-length λ plotted as a function of the extreme isopycnal displacement η_{ext} for density 1 with $a = 0.01$, $z_0 = 70$ and $d = 10$. Dashed line: KdV model results.	47
4.8	Vertical profiles of horizontal velocity u for $A = 0.1, 0.25, 0.5, 1, 2, 3, 4, 5, 7, 10, 15, 20, 25, 30, 50, 70, 100, 120$ and for conjugate flow solution. Dotted line: fully nonlinear model results; solid line: conjugate flow model solution. Dotted lines for $A = 50, 70, 100, 120$ are indistinguishable from the solid curve.	48
4.9	Density contours for $A = 25$ at (a) $t = 0$ and (b) $t = 20$ hours. Wave is propagating to left.	50

4.10	Density contours for $A = 100$ at (a) $t = 0$ and (b) $t = 20$ hours. Wave is propagating to left.	51
4.11	Density contours for $A = 100$ at (a) $t = 0$ and (b) $t = 20$ hours with higher numerical resolution. Wave is propagating to left.	52
5.1	Variation of η_{ext} as a function of z_0 in the Boussinesq case for $d = 5$ (solid line), $d = 10$ (dashed line), and $d = 15$ (dash dotted line).	58
5.2	η profiles for $d = 10$ in the Boussinesq case. $z_0 = 80, 70, 60, 52, 48, 40, 30, 20$ from left to right.	59
5.3	η profiles plotted as a function of $z - \eta(z)$. Same cases as in Figure 5.2. $z_0 = 80, 70, 60, 52, 48, 40, 30, 20$ from left to right.	59
5.4	η_{ext} for conjugate flow solution plotted as a function of z_0 for $a = 0.01$ (dotted line), $a = 0.1$ (dashed line) and $a = 0.5$ (dash dotted line) in the non-Boussinesq case. Solid lines are the Boussinesq approximation results. (a) $d = 5$, (b) $d = 10$, (c) $d = 15$	61
5.5	Density profiles in (a) undisturbed and (b) disturbed density fields with the Boussinesq approximation for $a = 0.01$, $d = 10$, $z_0 = 80$ (solid line), 70 (dashed line), 60 (dash dotted line), 52 (dotted line).	62
5.6	Same cases as Figure 5.5 for N^2 profiles.	63
5.7	Variation of phase speed c as a function of z_0 for $a = 0.01$ and $d = 5, 10, 15$ in the Boussinesq (solid line) and non-Boussinesq (dashed line) cases. The latter are indistinguishable from the former at this scale.	64

5.8	Phase speed c plotted as a function of z_0 for $a = 0.1$. Solid line: with the Boussinesq approximation; dashed line: without the Boussinesq approximation.	65
5.9	Same as Figure 5.8 for $a = 0.5$	65
5.10	Comparison of phase speed c as a function of z_0 for $d = 10$. (a) $a = 0.01$. (b) $a = 0.1$. (c) $a = 0.5$. Curves are for the non-Boussinesq case (dashed line), the Boussinesq case with the average value of the surface and bottom densities as the reference density (solid line) and with the vertically mean density as the reference density (dash dotted line).	67
5.11	Horizontal velocity $u(z)$ profile at the centre of flat-centred internal solitary wave for $a = 0.01$, $d = 10$ with the Boussinesq approximation. $z_0 = 20, 30, 40, 48, 52, 60, 70, 80$ from left to right in the upper half.	68
5.12	The breaking curves $z_l(d)$ and $z_u(d)$ and contours of minimum Richardson number for density 1. Curves are for Boussinesq case (solid) and non-Boussinesq cases for $a = 0.01$ (dashed) and $a = 0.1$ (dots).	71
5.13	Density (a) and N^2 (b) profiles for $z_0 = 70$ and $d = 10, 100, 1000$. In (b), the dashed line and solid line are with and without the Boussinesq approximation, respectively.	73

5.14	η_{ext} (a), c (b), $\eta'(0)$ (c), and $\eta'(H)$ (d) versus d for $z_0 = 60$ in the second density field for the Boussinesq (solid line) and non-Boussinesq (dashed line) cases.	74
5.15	η_{ext} (a), c (b), $\eta'(0)$ (c), and $\eta'(H)$ (d) versus d for $z_0 = 70$ in the second density field for the Boussinesq (solid line) and non-Boussinesq (dashed line) cases.	75
5.16	$\eta(z)$ profiles for $z_0 = 70$. $d = 70, 60, 50, 40$ from left to right. Solid lines: non-Boussinesq case; dashed lines: Boussinesq case.	76
5.17	$\eta_z(z)$ profiles for $z_0 = 70$. $d = 40, 50, 60, 70$ from left to right in the upper part. Solid lines: non-Boussinesq case; dashed lines: Boussinesq case.	76
6.1	Density $\bar{\rho}$ (a) and N^2 (b) profiles for density 2 with $a_1 = a_2 = 0.01$, $d_1 = d_2 = 10$, $z_1 = 20$, $z_2 = 80$ with the Boussinesq approximation.	79
6.2	Variation of η_{ext} as a function of z_1 for density 2 with $a_1 = a_2 = 0.01$, $d_1 = d_2 = 10$, $z_2 = H - z_1$. Solid line: Boussinesq approximation; dashed line: without the Boussinesq approximation.	80
6.3	Density (a) and N^2 (b) profiles in undisturbed (solid line) and disturbed (dashed line) regions for density 2 with $a_1 = a_2 = 0.01$, $d_1 = d_2 = 10$ and $z_1 = 32.44$ ($z_2 = H - z_1$).	81

6.4	Propagation speed c plotted as a function of z_1 . Same cases as in Figure 6.2. Curves are for Boussinesq case (solid line) and non-Boussinesq case for depressed wave (dashed line) and elevated wave (dash dotted line).	82
6.5	Variations of η_{ext} as a function of z_1 for density 2 for various values of z_2 . $a_1 = a_2 = a$ and $d_1 = d_2 = 10$. Solutions for the Boussinesq case (solid line) and non-Boussinesq cases for $a = 0.01$ (dashed line) and $a = 0.1$ (dash dotted line) are shown.	85
6.5	Continued	86
6.6	Joining of solution branches for density 2 when η_{ext} is plotted as a function of z_1 . $a_1 = a_2$, $d_1 = d_2 = 10$. Boussinesq case (solid line) and non-Boussinesq case for $a = 0.01$ (dashed line). (a) $z_2 = 67.6$; (b) $z_2 = 67.7$	87
6.7	Propagation speed c as a function of z_1 for density 2 with the Boussinesq approximation. $a_1 = a_2 = a$, $d_1 = d_2 = 10$. Solid lines correspond to the main solution branches. For $z_2 = 60, 65$, the dashed/dotted lines correspond to the upper/lower part of the left solution branch. For $z_2 = 70, 75, 80$, the dashed/dotted lines correspond to the upper/lower part of the upper solution branch.	88
6.7	Continued	89

- 6.8 Dependence of η_{ext} on d for density 2 in the Boussinesq case. Plotted as a function of z_1 for $z_2 = 60$ (a) and $z_2 = 80$ (b). $a_1 = a_2 = 0.01$. $d_1 = d_2 = 5$ (solid line), 10 (dashed line) and 15 (dash dotted line). 90
- 6.9 Variation of η_{ext} (a) and propagation speed c (b) as a function of z_1 for density 2 with $d_1 = d_2 = 10$. $a_1 = 0.1$, $a_2 = 0.01$. $z_2 = H - z_1$. Solid line: Boussinesq case; dashed line: non-Boussinesq case. 91
- 6.10 η_{ext} plotted as a function of z_1 for density 2 with $d = 10$ in the non-Boussinesq case for $z_2 = 20$ (solid line), 60 (dashed line), 80 (dash dotted line). Dotted line is the result when only the stronger pycnocline presents. (a) $a_1 = 0.01$, $a_2 = 0.1$; (b) $a_1 = 0.1$, $a_2 = 0.01$ 92
- 6.11 Propagation speed c versus z_1 for density 2 with $d = 10$ in the non-Boussinesq case for $z_2 = 20$ (solid line), 60 (dashed line), 80 (dash dotted line). (a) $a_1 = 0.01$, $a_2 = 0.1$; (b) $a_1 = 0.1$, $a_2 = 0.01$ 93
- 6.12 Variation of η_{ext} as a function of z_1 for density 2 when the largest density gradient of one pycnocline is double that of the other for $z_2 = 60$ and 80 in the non-Boussinesq case (solid lines). Panels (a), (b): $a_1 = 0.01$, $a_2 = 0.02$; panels (c), (d): $a_1 = 0.02$, $a_2 = 0.01$. The dashed lines are the results when only the stronger pycnocline exists. 94

6.13	Variation of η_{ext} as a function of z_1 for density 2 with $a_1 = a_2 = 0.01$ and $z_2 = 60$ without the Boussinesq approximation. Panels (a), (c), (e): d_1 fixed and $d_2 = 5$ (solid line), 10 (dashed line) and 15 (dash dotted line); panels (b), (d), (f): d_2 fixed and $d_1 = 5$ (solid line), 10 (dashed line) and 15 (dash dotted line).	97
6.14	Variation of η_{ext} as a function of z_1 for density 2 with $a_1 = a_2 = 0.01$ and $z_2 = 80$ without the Boussinesq approximation. Panel (a), (c), (e): d_1 fixed and $d_2 = 5$ (solid line), 10 (dashed line) and 15 (dash dotted line); panels (b), (d), (f): d_2 fixed and $d_1 = 5$ (solid line), 10 (dashed line) and 15 (dash dotted line).	98
6.15	$\eta(z)$ profiles showing the three conjugate flow solutions for density 2 with $a_1 = a_2 = 0.01$, $d_1 = d_2 = 10$, $z_1 = 30$, $z_2 = 80$.	100
6.16	Solitary wave corresponding to the elevation solution in Figure 6.15.	100
6.17	Solitary wave corresponding to the larger depression solution in Figure 6.15.	101
6.18	Solitary wave corresponding to the depression solution for the case $z_1 = 10$, $z_2 = 60$ using $d = 10$.	101

Chapter 1

Introduction

Internal waves occur in density stratified fluids due to gravitational restoring forces acting on vertically displaced fluid. They are ubiquitous features of the ocean and atmosphere. An internal solitary wave (ISW) is a special kind of internal wave. It is a vertically trapped wave propagating in the horizontal that arises because of a balance between linear dispersive and nonlinear processes in the fluid (Osborne and Burch, 1980). Internal solitary waves have many important properties, one of which is that they propagate with permanent shapes and speeds. The phase speed of the nonlinear internal solitary wave exceeds the associated linear long wave phase speed c_0 , and larger solitary waves travel faster than smaller ones. In the past several decades, great advances have been achieved in the general theory of nonlinear internal solitary waves, including the development of an asymptotic theory.

The generation of internal solitary waves strongly depends on the geographic area

and local conditions. Most are generated by tidal flow over topography. In a density stratified sea the tidal motion over a ridge or slope continually disturbs the pycnocline, thus creating an internal tide which travels away from the area of generation. If the internal tide is sufficiently large nonlinear effects cause wave steepening and then dispersive effects result in the formation of a number of shorter higher frequency waves including internal solitary waves.

Oceanic observations of internal solitary waves have often been reported. The observations of solitary waves were first accomplished primarily in inland seas and lakes or in the shallow regions of a shelf area (Ostrovsky and Stepanyants, 1989). In shallow water regions, the stratification often has a pronounced two-layer character: the lower layer may be either thicker or thinner than the upper one. If the upper layer is thinner (thicker) the internal solitary wave is a depression (elevation) (Keulegan, 1953). In the 1970s, Apel et al. (1975a, 1975b) reported how a subsurface wave can be observed from a satellite because surface waves interact with the surface current of internal waves which produces bands of choppy or calm water. The in situ measurements in the coastal region off New York showed that the maximum vertical isopycnal displacements were about 15 m. They argued that the waves were generated by semi-diurnal tidal flow at the shelf break and appeared as shoreward propagating packets of solitary-like waves 20–25 km apart. Sandstrom and Elliott (1984) observed solitary waves generated by the internal semi-diurnal tide on the shelf edge of the Atlantic coast off Nova Scotia, Canada. In each tidal cycle on the average two solitary waves

shaped like Korteweg-de Vries (KdV) solitons could be distinguished. In some cases there were four solitary waves of this type. The solitary waves were moving from the open sea toward the coast at a speed of about 1 m/s. Cummins and LeBlond (1984) presented the experimental observations of internal solitary waves in the Davis Strait on the Atlantic coast of northern Canada. Their data showed about 20 solitary waves shaped like KdV solitons. The characteristic length scale at half of the maximum amplitude value of the internal solitary waves was 250–275 m. Based on the satellite image data, Fu and Holt (1984) reported that there may be 20 internal solitary waves generated in the Gulf of California in one tidal cycle. Numerical simulations have shown that internal waves observed near the Georges Bank were generated by strong tidal flow across the bank edge (Lamb, 1994). Nagovitsyn and Pelinovsky (1988) observed internal solitary waves in the shelf zone of the Okhotsk Sea from a vessel moored at a depth of 70 m using three separately distributed temperature sensors 20 m long. Their experiments were carried out for 10 days in the summer of 1986 with a maximum continuous cycle of measurements of 52 hours. The internal solitary waves were observed to move from the open sea toward the coast. A total of 45 internal waves were registered, with a typical amplitude of 5 - 10 m, and a spatial scale of 200 - 400 m. Halpern (1971 a,b), Haury et al. (1979), and Chereskin (1983) also reported the observations of internal solitary waves in Massachusetts Bay.

Internal solitary waves not only exist in shallow water, but also in deep waters up to hundreds of kilometres from the shelf (Ostrovsky and Stepanyants, 1989). Osborne

and Burch (1980) observed large amplitude, long internal solitary waves in the Andaman Sea which has a depth of 1093 m. They found that the internal solitary waves occurred in packets of rank-ordered waves, the largest leading the rest. The packets occurred every 12 hours and 26 minutes, which indicated a tidal origin for the internal solitary waves. Apel et al. (1985) and Liu et al. (1985) reported internal solitary waves in the Sulu Sea. After analyzing the observations and the dynamics of internal solitary waves from their birth to decay at the coastal shelf, both Apel et al. (1985) and Liu et al. (1985) point out that tidal waves produce an initial perturbation which gradually becomes steeper, forms an undular bore, and then decomposes into a group of about six solitary waves. This result is identical to that of Osborne and Burch (1980). Pingree and Mardell (1985) found internal solitary waves in the Celtic Sea. Their observations showed that internal solitary waves appear both on the seasonal and on the main permanent pycnocline. Their propagation velocities vary from 1 m/s to 2.5 m/s; they are essentially depressions of a pycnocline with amplitudes of 20–100 m and more. Their characteristic lengths vary between 200 and 3000 m.

Many theories have been developed in the study of vertically trapped horizontally propagating internal waves. The most widely used theory is weakly nonlinear theory which assumes that the amplitude of the internal wave is small compared to the water depth and that the wave is long compared to a vertical length scale. Three different theories have been developed according to the relative sizes of the fluid depth H , a length scale h measuring the thickness of pycnocline, and wavelength L

(Koop & Butler, 1981). Each theory yields a different evolution equation to describe the temporal and horizontal structure of the wave. Shallow-water theory (Benjamin, 1966; Benney, 1966) has $H/L \ll 1$ and $h/H = O(1)$ and results in the Korteweg-de Vries (KdV) equation. Deep water theory has $H/L \gg 1$ and $h/L \ll 1$ and results in the Benjamin-Ono equation (Benjamin, 1967; Ono, 1975). The finite depth theory has $h/L \ll 1$ and $h/H \ll 1$ which results in the Joseph equation (Joseph, 1977; Kubota et al., 1978). These equations are the results of first-order theory and they all have exact solitary wave solutions. These solutions are approximate solutions which represent the dominant terms in an asymptotic expansion for the corresponding exact solution of the governing equations. Alternatively, large amplitude long waves in a weak stratification can be treated by similar asymptotic methods (Benney, 1978, 1982). In weakly nonlinear theories the principal small parameter ϵ used in the asymptotic analysis is a measure of the wave amplitude and is related to the ratio of the vertical to horizontal length scales of the waves. The balance of the nonlinear and dispersive terms gives the internal solitary wave solutions.

The theory of internal solitary waves was initiated by Keulegan (1953) and Long (1956). They considered a two-layer fluid with a small discontinuity in density and pointed out that the interfacial displacement is positive/negative if the upper layer is thicker/thinner than the lower layer. Benjamin (1966) and Benney (1966) derived the KdV equation by keeping the first order terms in the asymptotic expansion and obtained a solitary wave solution. It predicts that solitary waves travel faster than

linear long waves, and that as the wave amplitude increases the waves become narrower. The latter prediction is generally true only if the waves are not too large (Lamb, 1997). The validity of the theory decreases as either the wave amplitude increases or the wavelength decreases.

Observations of internal solitary waves show that moderate or large amplitudes are quite common. For these cases the modified KdV equation and generalized KdV equation have been derived by including the second-order terms of the asymptotic expansion (Lee and Beardsley, 1974; Miles, 1979, 1981; Gear and Grimshaw, 1983; Helfrich et al, 1984; Helfrich and Melville, 1986; Lamb and Yan, 1996). The inclusion of second-order terms significantly improves the agreement between the theory and experiments.

The weakly nonlinear theories are based on the assumption that the amplitude of a wave is small compared to the fluid depth. These theories are approximations to the fully nonlinear theory. In applications, the weakly nonlinear theories are often extrapolated into amplitude regimes where the assumptions under which they are derived are violated. Although it is remarkable that the predictions of weakly nonlinear theories for some flow quantities agree quite favorably with experimental data even for moderately large wave amplitudes, some notable discrepancies, both quantitative and qualitative, exist for other important flow quantities (Tung et al., 1982). For example, weakly nonlinear theories predict that the propagation speed of a solitary wave is linearly related to the wave amplitude. The experimental data of Davis and

Acrivos (1967) showed a definite and substantial slower rate of increase with amplitude as it passed the weakly nonlinear regime. Also, weakly nonlinear theories predict that the wavelength of the solitary wave decreases as wave amplitude increases, while studies of fully nonlinear solitary waves show that for some stratifications both the amplitude and the wavelength increase as wave energy increases (Tung et al., 1982; Turkington et al., 1991).

Tung et al.(1982) analyzed large amplitude internal solitary waves with the Boussinesq approximation using continuation methods and monotone iteration schemes. They proved analytically, and confirmed through numerical computations, that with the Boussinesq approximation large amplitude locally-confined mode-1 internal solitary waves are possible in a stratified fluid of finite depth. By using a variational formulation of the governing equations, Turkington et al.(1991) proposed a numerical technique for computing fully nonlinear solitary wave solutions in a stratified fluid, and presented several examples of mode-1 solitary waves. By studying the internal solitary waves in a density stratified fluid of shallow depth, Akylas and Grimshaw (1992) proved that solitary-like waves of mode higher than 1 actually develop oscillatory tails of infinite extent consisting of lower mode short waves. Thus Turkington's method (Turkington et al., 1991) can only compute mode-1 internal solitary waves.

For accurate evaluation of large amplitude internal waves, methods that do not assume a priori the isopycnal displacement, η , to be small compared to layer depth must be used. The question of "how large can internal solitary waves be?" is of

considerable interest in the oil industry because large internal solitary waves can affect oil rig production in marginal seas.

To find the maximum internal solitary wave for a given density stratification is also of the theoretical interest. Recently many researchers (Tung et al., 1982; Meiron and Saffman, 1983; Funakoshi and Oikawa, 1986; Grimshaw and Pullin, 1986; Pullin and Grimshaw, 1988; Turner and Vanden-Broeck, 1988; Turkington et al., 1991; Evans and Ford, 1996) have focused on large amplitude internal periodic and solitary waves and have discovered that for some stratifications (including the 2-layer case) the wave amplitude, measured in terms of the maximum isopycnal displacement or the maximum surface current, is bounded by an upper limit. Meiron and Saffman (1983) proved the existence of overhanging large amplitude internal gravity waves for a two-layer fluid. That is, the wave shows an *S*-shape in which heavy fluid lies above light fluid. As solutions of steady equations of motion, the *S*-shaped wave is probably unstable and does not exist in nature. Pullin and Grimshaw (1988) calculated the large amplitude waves of the overhanging forms in a two-layer fluid. They only considered periodic waves. This phenomenon seems to be only possible for periodic waves, as such behavior has not been found in work on internal solitary waves (Turner and Vanden-Broeck, 1988; Evans and Ford, 1996).

Using integral equation techniques Turner and Vanden-Broeck (1988) studied the internal solitary waves for a two-layer fluid confined in a channel of finite vertical and infinite horizontal extents. They argued that as the wave energy level increases, the

wave amplitude first increases, but then the most pronounced feature is a broadening of the wave while only a slight increase in amplitude takes place. The solitary wave becomes flat-topped (or flat-bottomed). As the waves become broader the amplitude and wave speed appear to approach limiting values. The flow in the broad midsection of the wave becomes uniform and horizontal. Benjamin (1966) termed such a flow “conjugate” to the uniform flow far upstream and downstream of the solitary wave (the outskirts flow). Using the exact potential flow integral equation approach, Evans and Ford (1996) studied two-layer internal solitary waves. They showed that the concept of a conjugate flow could be used to successfully predict the properties of the flow in the centre of a flat-topped wave in a two-layer fluid system.

The flow in the middle of a flat-centred internal solitary wave is conjugate to the far upstream flow. Thus, for a given stratification a flat-centred wave can exist only if there is a conjugate flow. Because it is much simpler to find a conjugate flow for a given stratification than it is to compute an internal solitary wave, in this thesis, the existence of conjugate flow solutions for a variety of continuously stratified density fields is investigated. We examine which kinds of density fields have conjugate flow solutions and explore the properties of those solutions. The results are useful for improving our understanding of when flat-centred internal solitary wave can occur.

The Boussinesq approximation is common in oceanographic applications as the total density variation is small. By this approximation, the density is replaced by a constant reference value ρ_0 in the momentum equations except when it is multiplied

by g . Concerns have been expressed about the validity of the Boussinesq approximation in the context of internal solitary waves. Long (1956) and Benjamin (1966) pointed out that the Boussinesq approximation may lead to serious errors for some stratifications. In our calculations, we examine cases with and without this approximation and make comparisons between the resulting conjugate flow solutions.

We also use the fully nonlinear computational method to compute the internal solitary waves with various amplitudes in a continuously stratified fluid. For large amplitude internal solitary waves, comparison is made between the results obtained from the fully nonlinear computational method and from the conjugate flow model.

The conjugate flow model is developed in Chapter 2. Chapter 3 describes the computational model for fully nonlinear internal solitary waves. Chapter 4 verifies that the flow in the centre of a flat-centred internal solitary wave is given by conjugate flow solutions. The results for single pycnocline density stratifications are given in Chapter 5 and the results for double pycnocline density stratifications in Chapter 6. Chapter 7 contains the summary and conclusion.

Chapter 2

Conjugate Flow Model

For a two-dimensional, incompressible, inviscid, non-diffusive fluid motion the governing equations are:

$$\rho(\vec{U}_t + \vec{U} \cdot \vec{\nabla} \vec{U}) = -\vec{\nabla} p - \rho g \hat{k}. \quad (2.1)$$

$$\rho_t + \vec{U} \cdot \vec{\nabla} \rho = 0, \quad (2.2)$$

$$\vec{\nabla} \cdot \vec{U} = 0. \quad (2.3)$$

$\vec{U}(x, z, t) = (u, w)$ is the velocity vector in the vertical plane with u the horizontal velocity in the x direction and w the vertical velocity in the upward z direction. $\vec{\nabla}$ is the gradient operator $(\frac{\partial}{\partial x}, \frac{\partial}{\partial z})$ and t is the time. ρ and p are the density and pressure, respectively. g is the gravitational acceleration and \hat{k} is the unit vector in the upward

direction. The rigid lid approximation is made on the surface at $z = H$, where H is the fluid depth.

Mathematical proofs of the existence of mode-1 internal solitary wave solutions of (2.1)–(2.3) exist (Tung et al., 1982; Turkington et al., 1991). Weakly nonlinear theory predicts that as the amplitudes of these waves increase they become narrower. In the fully nonlinear case this occurs for some stratifications. In this case solitary waves grow in amplitude until they break (streamlines become vertical and overturning). For other stratifications, the wavelength first decreases as the amplitude increases, but when the wave amplitude passes a certain value, both the wavelength and wave amplitude increase as the wave energy level increases. With further increases in the wave energy level, the most pronounced feature is the broadening of the wave: the wave amplitude measured in terms of the maximum isopycnal displacement is bounded by an upper limit. The internal solitary wave becomes flat-centred and the flow in the broad centre of the wave (midsection) becomes uniform and horizontal (Tung et al., 1982; Turner and Vanden-Broeck, 1988). Benjamin (1966) termed such a midsection flow to be “conjugate” to the uniform flow far from the wave (the outskirts flow). This conjugate flow concept was first proposed by Benjamin (1962a,b) with reference to swirling flows and was pointed out to be equally valid to heterogeneous fluids (Benjamin, 1962b). Turner and Vanden-Broeck (1988) predicted the limiting vertical structure in the midsection by computing the flow. The localized, non-uniform flow regions joining the uniform conjugate flow region and uniform outskirts regions were

termed as wave front or “fluid surge” regions (Turner and Vanden-Broeck, 1988). Evans and Ford (1996) applied the conjugate flow concept to a two-layer fluid and successfully predicted the amplitude and propagation speed of flat-topped or flat-bottomed internal solitary waves. We extend the notion to a continuously stratified fluid.

Consider a continuously stratified fluid with density $\bar{\rho}(z)$ and depth H in an undisturbed state and a steady flat-centred internal solitary wave propagating toward the right into a fluid at rest at phase speed c . Suppose the fluid velocity in the centre of a flat-centred internal solitary wave is $U(z)$. In a reference coordinate frame moving with the solitary wave at speed c , the flow field far ahead of the solitary wave front is given by

$$(u, w, \rho, p) \longrightarrow (-c, 0, \bar{\rho}(z), \bar{p}(z)) \quad (2.4)$$

while far behind the solitary wave front (at the centre of the flat-centred internal solitary wave) the perturbed flow is given by

$$(u, w, \rho, p) \longrightarrow (U(z) - c, 0, \bar{\rho}_p(z), \bar{p}_p(z)). \quad (2.5)$$

Defining $\eta(z)$ to be the vertical displacement of the isopycnal at height z behind the wave front, where the fluid velocity is $U(z) - c$, relative to its height ahead of the wave front, where the fluid velocity is $-c$, the isopycnals (or streamlines) passing through heights z and $z + dz$ in the conjugate flow region have heights $z - \eta(z)$ and

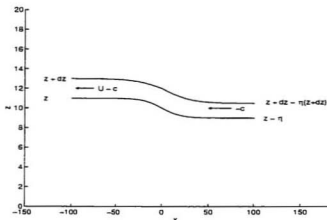


Figure 2.1: Geometrical interpretation of isopycnals passing through point (x, z) and $(x, z + dz)$ in the conjugate flow region.

$z + dz - \eta(z + dz)$ in the outskirts (see Figure 2.1). Thus, conservation of volume gives

$$(U(z) - c) \cdot (z + dz - z) = -c[z + dz - \eta(z + dz)] - [z - \eta(z)] \approx -c[dz - \eta'(z)dz] \quad (2.6)$$

or in the limit as $dz \rightarrow 0$,

$$U(z) = c \cdot \eta'(z). \quad (2.7)$$

The conservation of density gives

$$\bar{\rho}_p(z) = \bar{\rho}(z - \eta(z)). \quad (2.8)$$

Applying Bernoulli's theorem along an isopycnal with height z and $z - \eta(z)$ behind and ahead of the wave front respectively, gives

$$\begin{aligned} \frac{1}{2}\bar{\rho}_p(z)(U(z) - c)^2 + \bar{p}_p(z) + g\bar{\rho}_p(z)z = \\ \frac{1}{2}\bar{\rho}(z - \eta(z))c^2 + \bar{p}(z - \eta(z)) + g\bar{\rho}(z - \eta(z))(z - \eta(z)). \end{aligned} \quad (2.9)$$

Using (2.7) and (2.8) the above equation gives

$$\frac{c^2}{2}\bar{\rho}(z - \eta)[\eta'(\eta' - 2)] + \bar{p}_p(z) = \bar{p}(z - \eta) - g\bar{\rho}(z - \eta)\eta. \quad (2.10)$$

differentiating this equation with respect to z and using

$$\frac{d}{dz}(\bar{\rho}(z - \eta(z))) = \frac{d\bar{\rho}}{dz}(z - \eta(z))(1 - \eta'(z)). \quad (2.11)$$

gives

$$\begin{aligned} \frac{c^2}{2}\bar{\rho}'(z - \eta(z)) \cdot [1 - \eta'(z)][\eta'(z)(\eta'(z) - 2)] \\ + \bar{\rho}(z - \eta(z))c^2(\eta'(z) - 1)\eta''(z) \\ + \frac{d\bar{p}_p(z)}{dz} = \\ \frac{d\bar{p}}{dz}(z - \eta(z)) - g\bar{\rho}(z - \eta(z))\eta'(z) \\ - g\bar{\rho}'(z - \eta(z))[1 - \eta'(z)]\eta(z). \end{aligned} \quad (2.12)$$

The hydrostatic conditions give

$$\frac{d\bar{p}(z)}{dz} = -\bar{\rho}(z)g. \quad (2.13)$$

and

$$\frac{d\bar{p}_p(z)}{dz} = -g\bar{\rho}_p(z) = -g\bar{\rho}(z - \eta(z)). \quad (2.14)$$

Substituting (2.13) and (2.14) into (2.12) we have.

$$\frac{c^2}{2}\bar{\rho}'(z - \eta(z))\eta'(z)(\eta'(z) - 2) - c^2\bar{\rho}(z - \eta(z))\eta''(z) = -g\bar{\rho}'(z - \eta(z))\eta(z). \quad (2.15)$$

Denoting

$$N^2(z) = -\frac{g}{\bar{\rho}(z)}\frac{d\bar{\rho}}{dz}(z) \quad (2.16)$$

(2.15) becomes the following nonlinear eigenvalue problem for $\eta(z)$ and c :

$$\eta''(z) + \frac{N^2(z - \eta(z))}{2g}\eta'(z)(\eta'(z) - 2) + \frac{N^2(z - \eta(z))}{c^2}\eta(z) = 0 \quad (2.17)$$

with boundary conditions

$$\eta(0) = \eta(H) = 0. \quad (2.18)$$

The nonlinear eigenvalue problem (2.17)–(2.18) is solved numerically by a standard shooting method in which (2.17) is solved by the initial value method for initial

conditions $\eta(0) = 0$ and some guessed value of $\eta'(0)$. This results in a value $\eta(H)$ which depends on c . In general there is a discrepancy between the $\eta(H)$ value and the desired boundary condition. A root search is then done to determine c in order to satisfy the boundary condition. In general there are an infinite number of roots, or eigenvalues, for c corresponding to different modes. We focus on mode-1 waves only, in which case we take the largest eigenvalue. The corresponding solution $\eta(z)$ has no zeros between the bottom and the surface. For the linearized eigenvalue problem, by choosing any value of $\eta'(0)$ we get a solution $\eta(z)$ and $a \cdot \eta(z)$ is also a solution for any constant a . So that we are free to choose any nonzero value for $\eta'(0)$ in searching for the solution. This is not true for nonlinear eigenvalue problem (2.17)-(2.18) since here the solution depends on $\eta'(0)$. We need an auxiliary condition to determine the value of $\eta'(0)$, and this condition is obtained by considering the horizontal flow force in the fluid.

The horizontal flow force F acting on a vertical section of the system is equal to the horizontal pressure force plus the flux of horizontal momentum (Benjamin, 1966), that is

$$F = \int_0^H (pdz + \rho u^2 dz) \quad (2.19)$$

where p is pressure, ρ is density, and u is the velocity of the fluid. For a steady flow system, because there is no external horizontal force acting on the system, the horizontal flow force acting on any vertical section of the system is the same, i.e., F

is independent of x . This is easily proved, from (2.19) we have

$$\begin{aligned}\frac{dF}{dx} &= \int_0^H (p_x + (\rho u^2)_x) dz \\ &= \int_0^H (p_x + 2\rho u u_x + u^2 \rho_x) dz.\end{aligned}\tag{2.20}$$

By using the continuity equation

$$u_x + w_z = 0,\tag{2.21}$$

the above equation becomes

$$\begin{aligned}\frac{dF}{dx} &= \int_0^H (p_x + \rho u u_x - \rho u w_z + u^2 \rho_x) dz \\ &= \int_0^H [p_x + \rho(u u_x + w u_z)] dz + \int_0^H (\rho_z u w + u^2 \rho_x) dz \\ &= \int_0^H [p_x + \rho(u u_x + w u_z)] dz + \int_0^H u[u \rho_x + w \rho_z] dz.\end{aligned}\tag{2.22}$$

From the momentum conservation and mass conservation equation in a steady flow system, we know

$$p_x + \rho(u u_x + w u_z) = 0,\tag{2.23}$$

and

$$u \rho_x + w \rho_z = 0.\tag{2.24}$$

So that (2.22) becomes

$$\frac{dF}{dx} = 0. \quad (2.25)$$

The horizontal flow force is independent of x .

By setting F equal on the two vertical sections far ahead of the wave and at the wave centre we have, using $U(z) = c\eta'(z)$,

$$\int_0^H (c^2 \bar{\rho}(z - \eta(z))(\eta'(z) - 1)^2 + \bar{p}_b(z)) dz = \int_0^H (c^2 \bar{\rho}(z) + \bar{p}(z)) dz. \quad (2.26)$$

Changing the variable of integration for the right-hand side of (2.26) to s by $z = s - \eta(s)$, then $dz = (1 - \eta'(s))ds$ and using $s = 0$ when $z = 0$, $s = H$ when $z = H$, this side of the equation (2.26) becomes

$$\int_0^H (c^2 \bar{\rho}(z) + \bar{p}(z)) dz = \int_0^H (c^2 \bar{\rho}(s - \eta(s)) + \bar{p}(s - \eta(s))) [1 - \eta'(s)] ds. \quad (2.27)$$

If s is replaced by z , the right-hand side of equation (2.27) can be written as

$$\int_0^H (c^2 \bar{\rho}(z - \eta(z)) + \bar{p}(z - \eta(z))) [1 - \eta'(z)] dz. \quad (2.28)$$

Thus (2.26) becomes

$$\int_0^H (\bar{p}_r(z) - \bar{p}(z - \eta(z))[1 - \eta'(z)] - c^2 \bar{\rho}(z - \eta(z))[1 - \eta'(z)]\eta'(z)) dz = 0. \quad (2.29)$$

To simplify, we use η to represent $\eta(z)$ in the following equations. From (2.9) we have.

$$\bar{p}_p(z) - \bar{p}(z - \eta) = \frac{1}{2}c^2\bar{\rho}(z - \eta)\eta'[2 - \eta'] + g\bar{\rho}(z - \eta)[z - \eta] - g\bar{\rho}_p(z)z. \quad (2.30)$$

Substituting into (2.29), gives

$$\int_0^H \left(\bar{p}(z - \eta)\eta' + \frac{1}{2}c^2\bar{\rho}(z - \eta)\eta'(2 - \eta') - g\bar{\rho}(z - \eta)\eta - c^2\bar{\rho}(z - \eta)(1 - \eta')\eta' \right) dz = 0 \quad (2.31)$$

or

$$\int_0^H \bar{p}(z - \eta)\eta' dz + \int_0^H \left(\frac{1}{2}c^2\bar{\rho}(z - \eta)\eta'^2 - g\bar{\rho}(z - \eta)\eta \right) dz = 0. \quad (2.32)$$

Using integration by parts and the hydrostatic condition (2.14) the first term can be rewritten as

$$\int_0^H \bar{p}(z - \eta)\eta' dz = - \int_0^H \eta \frac{d\bar{p}}{dz}(z - \eta)(1 - \eta') dz = \int_0^H g\bar{\rho}(z - \eta)(1 - \eta')\eta dz. \quad (2.33)$$

Thus, equation(2.32) becomes

$$\int_0^H \left(g\bar{\rho}(z - \eta)\eta\eta' - \frac{1}{2}c^2\bar{\rho}(z - \eta)\eta'^2 \right) dz = 0. \quad (2.34)$$

Integrating by parts of the first term we have

$$\int_0^H g\bar{\rho}(z-\eta)\eta\eta' dz = \frac{1}{2} \int_0^H \eta^2(1-\eta')\bar{\rho}(z-\eta)V^2(z-\eta)dz. \quad (2.35)$$

The governing ODE (2.17) is now used to replace $V^2(z-\eta)\eta$ and then the right-hand side of (2.35) becomes

$$\begin{aligned} \int_0^H g\bar{\rho}(z-\eta)\eta\eta' dz &= -c^2 \int_0^H \frac{1}{2}\eta\bar{\rho}(z-\eta) \left(\eta' - \frac{\eta'^2}{2} \right)' dz \\ &\quad -c^2 \int_0^H \frac{1}{4}\bar{\rho}(z-\eta) \frac{V^2(z-\eta)}{g} \eta(1-\eta')\eta'(\eta'-2)dz \end{aligned} \quad (2.36)$$

Using the definition of $V^2(z-\eta)$ given by (2.16) and integrating the first term of the right-hand side by parts we get

$$\int_0^H g\bar{\rho}(z-\eta)\eta\eta' dz = c^2 \int_0^H \bar{\rho}(z-\eta) \left(\frac{\eta'^2}{2} - \frac{1}{4}\eta'^3 \right) dz. \quad (2.37)$$

Substituting (2.37) into (2.34) gives the auxiliary condition

$$\int_0^H \bar{\rho}(z-\eta(z))\eta'^3(z) dz = 0 \quad (2.38)$$

which $\eta(z)$ must satisfy.

Since $U(z) = c\eta'(z)$, the auxiliary condition (2.38) indicates that in a reference frame fixed with respect to the outskirts region, the kinetic energy flux is zero.

In order to find the solution we must find the root of

$$T(\eta'(0)) = \int_0^H \bar{\rho}(z - \eta(z)) \eta'^3(z) dz = 0. \quad (2.39)$$

Given a value of $\eta'(0)$, the eigenvalue problem is solved for c , $\eta(z)$ and $\eta'(z)$. With these solutions $T(\eta'(0))$ can be evaluated. The root search is done to find the value of $\eta'(0)$ for which $T(\eta'(0)) = 0$.

It is important to point out that the valid solution of $\eta(z)$ must satisfy the condition

$$\eta'(z) < 1 \quad (2.40)$$

because the streamlines, which pass z at the centre of the wave and $z - \eta(z)$ far ahead of the wave, are assumed to extend to $\pm\infty$. Thus $z - \eta(z)$ must be an increasing function of z , so

$$\frac{d}{dz}(z - \eta(z)) > 0 \quad (2.41)$$

i.e.,

$$1 - \eta'(z) > 0 \quad (2.42)$$

or

$$\eta'(z) < 1. \quad (2.43)$$

When $\eta'(z) = 1$ the breaking ($U(z) = c$) of the conjugate flow solution occurs.

If the Boussinesq approximation is applied, the problem simplifies considerably. The nonlinear eigenvalue problem (2.17) becomes

$$\eta''(z) + \frac{N^2(z - \eta(z))}{c^2} \eta(z) = 0 \quad (2.44)$$

with boundary condition

$$\eta(0) = \eta(H) = 0. \quad (2.45)$$

The auxiliary condition (2.39) used to determine $\eta'(0)$ becomes

$$T(\eta'(0)) = \int_0^H \eta^{\alpha}(z) dz = 0. \quad (2.46)$$

Chapter 3

Computational Model for Fully Nonlinear Internal Solitary Waves

3.1 Governing Equations

Turkington et al. (1991) developed a method for computing the exact steadily translating solitary wave solutions of the equations (2.1)–(2.3). In this chapter this method is discussed for the simpler case where the Boussinesq approximation is made. Under the Boussinesq approximation equations (2.1)–(2.3) are

$$u_x + w_z = 0, \quad (3.1)$$

$$\rho_t + u\rho_x + w\rho_z = 0, \quad (3.2)$$

$$\rho_0(u_t + uu_x + ww_z) = -p_x, \quad (3.3)$$

$$\rho_0(w_t + uw_x + ww_z) = -p_z - \rho g, \quad (3.4)$$

where x and z are the horizontal and vertical coordinates, respectively. ρ is density, and ρ_0 is the reference density. p is pressure and (u, w) are velocity components in horizontal and vertical directions, and $g = 9.81 m/s^2$ is the acceleration due to gravity. A streamfunction ψ is introduced which satisfies $u = \psi_z$, $w = -\psi_x$. Defining vorticity as $\sigma = u_z - w_x$, equation (3.2) can be written as

$$\rho_t + J(\rho, \psi) = 0 \quad (3.5)$$

where the notation $J(A, B) = A_x B_z - A_z B_x$. Manipulating the curl of equations (3.3) and (3.4) we have

$$\rho_0(\sigma_t + J(\sigma, \psi)) - J(\rho, gz) = 0. \quad (3.6)$$

For the nonlinear solitary wave, assume the solutions of (3.5) and (3.6) have the form $\rho = \rho(x - ct, z)$, $\sigma = \sigma(x - ct, z)$ for some positive wave propagation speed c . The fluid is bounded by a fixed boundary at $z = 0$ and $z = H$, respectively. The fluid domain

is $-\infty < x < +\infty$, $0 \leq z \leq H$. In a reference frame moving with the propagation speed c , the motion is steady and equations (3.5) and (3.6) reduce to

$$J(\rho, v - cz) = 0. \quad (3.7)$$

$$\rho_0(J(\sigma, v - cz)) - J(\rho, gz) = 0. \quad (3.8)$$

The propagation speed c is unknown and needs to be determined as part of the solution.

The undisturbed density stratification of the fluid at $x = \pm\infty$ is specified by a function $\bar{\rho}(z)$ satisfying

$$\bar{\rho}(z) > 0, \quad \bar{\rho}'(z) < 0 \quad (0 \leq z \leq H). \quad (3.9)$$

A solitary wave disturbance is a solution of (3.8) satisfying the asymptotic conditions

$$\rho(x, z) \rightarrow \bar{\rho}(z), \quad \sigma(x, z) \rightarrow 0, \quad v(x, z) \rightarrow 0, \quad \text{as } |x| \rightarrow \infty. \quad (3.10)$$

For the study of solitary waves we impose a restriction that every isopycnal surface ($\rho(x, z) = \text{constant}$) must connect to $x = -\infty$ and $x = +\infty$, or equivalently, that there are no closed isopycnal surfaces (entrained eddies). The isopycnal displacement $\eta(x, z)$ at point (x, z) represents the vertical displacement of the isopycnal surface

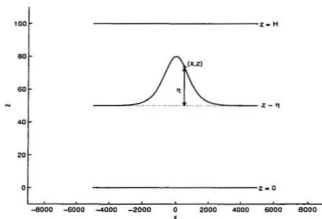


Figure 3.1: Geometrical interpretation of the vertical displacement $\eta(x, z)$ of an isopycnal surface passing through a point (x, z) .

passing through the point (x, z) from its undisturbed level as $x \rightarrow \pm\infty$. Hence, the density in the disturbed region can be represented by the density in the undisturbed region (Figure 3.1) via,

$$\bar{\rho}(x, z) = \bar{\rho}(z - \eta(x, z)). \quad (3.11)$$

A wave of elevation (depression) is represented by $\eta > 0$ ($\eta < 0$) in the domain. $\eta = 0$ at the upper and bottom boundaries and $\eta \rightarrow 0$ as $x \rightarrow \pm\infty$.

The (ρ, σ) system in (3.5) and (3.6) may be expressed in terms of η . Note that

$$J(f(A), B) = f'(A)J(A, B) = J(A, f'(A)B) \quad (3.12)$$

and using (3.11), equation (3.7) yields

$$\begin{aligned} J(\bar{\rho}(z - \eta), \psi - cz) &= \bar{\rho}'(z - \eta)J(z - \eta, \psi - cz) \\ &= \bar{\rho}'(z - \eta)J(z - \eta, \psi - c\eta - c(z - \eta)) = 0. \end{aligned} \quad (3.13)$$

Now

$$\begin{aligned} J(z - \eta, \psi - c\eta - c(z - \eta)) &= J(z - \eta, \psi - c\eta) - cJ(z - \eta, z - \eta) \\ &= J(z - \eta, \psi - c\eta). \end{aligned} \quad (3.14)$$

so that (3.13) gives

$$J(z - \eta, \psi - c\eta) = 0. \quad (3.15)$$

This implies that

$$R(z - \eta) = \psi - c\eta. \quad (3.16)$$

Now

$$\psi \rightarrow 0, \quad \eta \rightarrow 0 \quad \text{as} \quad x \rightarrow \infty. \quad (3.17)$$

Using this in (3.16) we have

$$R(z) = 0 \quad (3.18)$$

for all z so that (3.16) gives

$$\psi = c\eta. \quad (3.19)$$

Equation (3.8) is now reduced to

$$\begin{aligned} -\rho_0 c J(\sigma, \eta - z) + \bar{\rho}'(z - \eta) J(z - \eta, g z) &= J(z - \eta, -\rho_0 c \sigma + \bar{\rho}'(z - \eta) g(z - \eta + \eta)) \\ &= J(z - \eta, -\rho_0 c \sigma + \bar{\rho}'(z - \eta) g \eta) = 0 \end{aligned} \quad (3.20)$$

from which follows

$$J(z - \eta, -\rho_0 c \sigma + \bar{\rho}'(z - \eta) g \eta) = 0. \quad (3.21)$$

So that

$$-\rho_0 c \sigma + \bar{\rho}'(z - \eta) g \eta = G(z - \eta). \quad (3.22)$$

Setting $x \rightarrow \pm\infty$ in (3.22) and using $\sigma \rightarrow 0$ and $\eta \rightarrow 0$ as $x \rightarrow \pm\infty$ we get $G = 0$ for all z , so that

$$-\rho_0 c \sigma + \bar{\rho}'(z - \eta) g \eta = 0. \quad (3.23)$$

or

$$\frac{\sigma}{c} = \frac{g}{\rho_0 c^2} \eta \bar{\rho}'(z - \eta). \quad (3.24)$$

Combining (3.19) and (3.24) and using $\sigma = \nabla^2 \psi$, the nonlinear eigenvalue problem

becomes (Turkington et al., 1991)

$$\nabla^2 \eta = \lambda \frac{\eta}{\rho_0 H} \bar{\rho}'(z - \eta) \quad (3.25)$$

where the eigenvalue parameter is defined by

$$\lambda = \frac{gH}{c^2} \quad (3.26)$$

and $\bar{\rho}(z)$ is the density profile far from the wave. Equation (3.25) simplifies to equation (2.44) if η depends only on z . The boundary conditions are

$$\eta = 0 \quad \text{at} \quad z = 0, H. \quad (3.27)$$

$$\eta \rightarrow 0 \quad \text{as} \quad x \rightarrow \pm\infty. \quad (3.28)$$

The iteration procedure used by Turkington et al. (1991) to solve (3.25)–(3.28) is based on a variational formulation of the problem. Equations (3.25)–(3.28) are precisely those that we use when a streamline displacement, $\eta(x, z)$, is sought which minimizes the kinetic energy subject to the constraint $F(\eta)$ takes on a prescribed value. Define

$$F(\eta) = \int \int_R f(z, \eta) dx, dz, \quad (3.29)$$

where

$$f(z, \eta) = \frac{1}{\rho_0 H} \int_0^\eta [\bar{\rho}(z - \eta) - \bar{\rho}(z - \xi)] d\xi \quad (3.30)$$

$F(\eta)$ is proportional to a potential energy. The value of $F(\eta)$ will be denoted by A . It will be used to define the wave amplitude in the remainder of this thesis.

The iteration procedure can be divided into the following steps:

(I). Give the value of A which determines the amplitude and wavelength of the internal solitary wave.

(II). Estimate the initial value η^0 .

(III). Solve

$$\nabla^2 W^k = \frac{\eta^k}{\rho_0 H} \bar{\rho}'(z - \eta^k) \quad (3.31)$$

$$W^k = 0 \text{ on } z = 0, H$$

$$W^k \rightarrow 0 \text{ as } x \rightarrow \pm\infty.$$

$$\text{where } k = 0, 1, 2 \dots$$

(IV). Evaluate integrals

$$F(\eta^k) = \int \int f(z, \eta^k) dx dz \quad (3.32)$$

$$S_1 = -\frac{1}{\rho_0 H} \int \int \bar{\rho}'(z - \eta^k) \eta^k W^k dx dz \quad (3.33)$$

$$S_2 = -\frac{1}{\rho_0 H} \int \int \bar{\rho}'(z - \eta^k) (\eta^k)^2 dx dz. \quad (3.34)$$

(V). Define

$$\lambda^{k+1} = \max \left\{ 0, \frac{A - F(\eta^k) + S_2}{S_1} \right\}. \quad (3.35)$$

(VI). Update

$$\eta^{k+1} = \lambda^{k+1} W^k. \quad (3.36)$$

Assuming convergence as $k \rightarrow \infty$ it is easily seen that

$$S_2 = \lambda^\infty S_1, \quad (3.37)$$

$$\lambda^\infty = \max \left(\frac{A - F(\eta^\infty)}{S_2} + \lambda^\infty \right). \quad (3.38)$$

This gives

$$F(\lambda^\infty) = A \quad (3.39)$$

and η^∞ solves equation (3.25) with $\lambda = \lambda^\infty$.

Once the eigenvalue λ and eigenfunction η are determined, the nonlinear phase speed of the wave c and streamfunction ψ can be obtained easily.

$$c = \sqrt{\frac{gH}{\lambda}} \quad (3.40)$$

$$\psi = c\eta. \quad (3.41)$$

Thus, the horizontal and vertical velocity of the fluid can be expressed as

$$u = c\eta_z, \quad (3.42)$$

and

$$w = -c\eta_x. \quad (3.43)$$

3.2 Numerical Method

Equation (3.31) is the Poisson equation; for a given density field, the right-hand side of the equation is known. There are many methods to solve the Poisson equation (Hockney, 1965; Buneman, 1969; Dorr, 1970), but we use the direct marching method (Roache, 1978). The basic idea is to solve a boundary value problem with split boundary conditions, by guessing the missing conditions at one boundary and marching the solution, as an initial value problem, to the second boundary. The resulting final values at the end of the march are compared with the desired boundary values, and on that basis the guessed conditions are corrected and the march is repeated for the final correct solution. For linear equations, the correction can be exact and only two marches are required to obtain the solution. This method is commonly used for ordinary differential equations. Roache (1978) proved that this method can also be applied to Poisson elliptic equations and is stable if a cell aspect ratio $\Delta x/\Delta z > 1$, where Δx and Δz are the grid spacing in the x and z directions, respectively.

To simplify, equation (3.31) can be written in the form of

$$\nabla^2 W \equiv \frac{\partial^2 W}{\partial x^2} + \frac{\partial^2 W}{\partial z^2} = f(x, z). \quad (3.44)$$

We consider a rectangular domain bounded below by $z = 0$ and above by a rigid lid at $z = H$ and $x = \pm L$ at the left and right boundaries. The domain is divided into I evenly spaced grid cells in x direction and J grid cells in z direction. The boundary conditions are

$$\eta = 0 \quad \text{at} \quad z = 0, H, \quad (3.45)$$

$$\eta = 0 \quad \text{at} \quad x = \pm L. \quad (3.46)$$

The second-order accurate, five-point finite differencing scheme is

$$\frac{W_{i+1,j} - 2W_{i,j} + W_{i-1,j}}{\Delta x^2} + \frac{W_{i,j+1} - 2W_{i,j} + W_{i,j-1}}{\Delta z^2} = f_{i,j} \quad (3.47)$$

where Δx is grid space in x direction and Δz is grid space in z direction. The boundary condition is $W = 0$ at upper and bottom as well as left and right boundaries.

First, it is necessary to pick an arbitrary vector of provisional values $W'_{i,1}$ just inside the bottom boundary, say $W'_{i,1} = W_{i,0}$. This $W'_{i,1}$ is in error by the error vector $e_{i,1}$:

$$W_{i,1} = W'_{i,1} + e_{i,1}. \quad (3.48)$$

With $W'_{i,1}$ so chosen, the remaining provisional values for $1 \leq i \leq (I-1)$ and j up to J (surface boundary) are calculated in one march starting at $(i,2)$. Equation (3.47) can be rearranged as:

$$W'_{i,j+1} = \Delta z^2 f_{i,j} + (2 + 2\alpha)W'_{i,j} - \alpha(W'_{i+1,j} + W'_{i-1,j}) - W'_{i,j-1} \quad (3.49)$$

where $\alpha = (\Delta z / \Delta x)^2$. The correct boundary values of $W_{0,j}$ at the left boundary and $W_{I,j}$ at the right boundary are used in equation (3.49) when needed. The error propagation equation is then

$$e_{i,j+1} = -\alpha e_{i-1,j} + (2 + 2\alpha)e_{i,j} - \alpha e_{i+1,j} - e_{i,j-1} \quad (3.50)$$

with boundary values along the bottom, left and right boundaries of

$$e_{i,0} = e_{0,j} = e_{I,j} = 0. \quad (3.51)$$

After the first march of $W'_{i,j}$, the values of the final error vector $e_{i,J}$ are calculated from

$$e_{i,J} = W_{i,J} - W'_{i,J} \quad (3.52)$$

where $W_{i,J}$ is zero (this is the known boundary).

From equation (3.50) a linear relation between $e_{i,J}$ and $e_{i,1}$ may be established.

allowing the solution for $e_{i,1}$ in terms of $e_{i,j}$. With $e_{i,1}$ known, the correct values of $W_{i,1}$ are obtained from (3.48) and a second march using the recursive relation equation (3.49) (with W replacing W') establishes the final solutions.

The method to relate $e_{i,1}$ and $e_{i,j}$ is as follows: from equation (3.50) we have

$$E_{j+1} = C \cdot E_j - E_{j-1} \quad (3.53)$$

where $E_j = \{e_{i,j}\}, i = 1, 2, \dots, I-1$, and

$$C = \begin{pmatrix} 2 + 2\alpha & -\alpha & 0 & \cdot & \cdot & 0 \\ -\alpha & 2 + 2\alpha & -\alpha & 0 & \cdot & 0 \\ 0 & -\alpha & 2 + 2\alpha & -\alpha & 0 & 0 \\ \cdot & \cdot & \cdot & \cdot & \cdot & \cdot \\ \cdot & \cdot & \cdot & \cdot & \cdot & \cdot \\ 0 & \cdot & \cdot & \cdot & -\alpha & 2 + 2\alpha \end{pmatrix} \quad (3.54)$$

is a tridiagonal matrix.

We can also relate E_j and E_1 in the form

$$E_j = C_j E_1. \quad (3.55)$$

From (3.53) and (3.55) we know that

$$E_2 = C E_1 - E_0 = C_2 E_1. \quad (3.56)$$

so that

$$C_2 = C. \quad (3.57)$$

Similarly, we can get

$$E_3 = C E_2 - E_1 = (C \cdot C_2 - I) E_1 \quad (3.58)$$

so

$$C_3 = C \cdot C_2 - I = C^2 - I. \quad (3.59)$$

In general we have

$$E_j = C E_{j-1} - E_{j-2} = (C \cdot C_{j-1} - C_{j-2}) E_1 \quad (3.60)$$

so that the general formula for C_j is

$$C_j = C C_{j-1} - C_{j-2}. \quad (3.61)$$

Since E_j is known and C_j is known we can solve

$$E_j = C_j E_1. \quad (3.62)$$

to get E_1 .

Chapter 4

Verification that the Flow in the Centre of a Flat-Centred Internal Solitary Wave is Given by the Conjugate Flow Solutions

In this chapter, we use the computational model discussed in Chapter 3 to compute internal solitary waves for a variety of wave amplitudes. A continuously stratified fluid for which flat-centred waves form at large amplitude is used. The purpose is to show how the flow in the centres of these waves converges to the conjugate flow solutions.

4.1 Model Initialization

The fully nonlinear model is solved in a rectangular domain bounded below by $z = 0$ and above by a rigid lid at $z = H$ and $x = \pm L$ at the left and right boundaries. The domain is evenly divided into I grid cells in the horizontal (x) direction and J grid cells in the vertical (z) direction.

The background state consists of a stably stratified fluid at rest. The density is nondimensionalized and scaled by a typical value of 1000 kg/m^3 , so that the nondimensional density is around 1. Other quantities are nondimensionalized by a length scale of 1 m and a time scale of 1 s . The first density (density 1) profile we used in our study is a single pycnocline density stratification, given by

$$\bar{\rho}(z) = 1.0 - a \cdot \tanh\left(\frac{z - z_0}{d}\right), \quad (4.1)$$

where z_0 represents the centre of the pycnocline, d the thickness of the pycnocline, and a/d the strength of the density stratification. With different a , z_0 and d values, the above formula gives different density profiles. The density and buoyancy frequency profiles with $a = 0.01$, $z_0 = 70$, and $d = 10$ are given in Figures 4.1 and 4.2.

In our model simulation, the nondimensional water depth is $H = 100$ and L is set to be 5000 initially. After we compute the wave we compare L and the wave half-length. L should be at least four times that of the wave half-length. The wave half-length is the horizontal width measured from the wave centre to the location

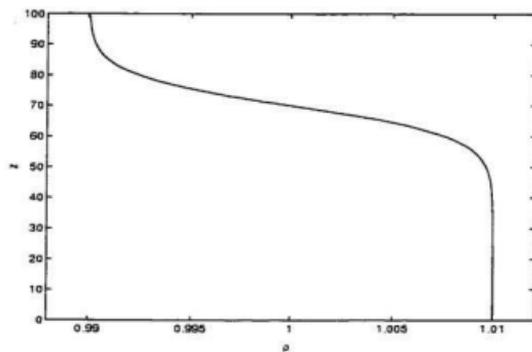


Figure 4.1: Density profile for density 1 with $a = 0.01$, $z_0 = 70$ and $d = 10$.

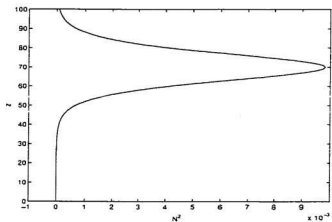


Figure 4.2: Buoyancy frequency profile for density 1 with $a = 0.01$, $z_0 = 70$ and $d = 10$.

where the surface horizontal velocity is one-half its maximum value. The coordinate system is set up such that the centre of the initial wave is at $x = 0$. The largest buoyancy frequency for this density stratification occurs at $z = z_0$. If $z_0 > 50$, the internal solitary wave is a wave of depression; if $z_0 < 50$, it is a wave of elevation. According to the weakly nonlinear theory, if $z_0 = 50$ there is no internal solitary wave. The value of A , which determines the extreme isopycnal displacement η_{ext} and wave half-length, is chosen before the calculation. For small A values, i.e. small amplitude waves, we initialized our model based on the KdV approximation. For large A values, the model is initialized by giving a wider wave. The initial guessed value of $\eta(x, z)$ will not affect the final result, even with a poor initial guess. Nevertheless, it affects the speed of convergence.

The boundary conditions are

$$\eta = 0 \quad \text{at} \quad z = 0, H. \quad (4.2)$$

$$\eta = 0 \quad \text{at} \quad x = \pm L. \quad (4.3)$$

(4.3) is an approximation to the correct boundary conditions for a solitary wave, namely that $\eta \rightarrow 0$ as $x \rightarrow \pm\infty$. Thus, the left and right boundary conditions will introduce a small error into the final results. This error, which will be discussed later, can be made smaller by increasing the domain size L .

The stopping criterion of the iterative algorithm in our computation is

$$\max(|\eta^{k+1} - \eta^k|) < 5 * 10^{-5} \quad (4.4)$$

in the whole domain, where η^k is the solution after k iterations.

4.2 Model Results

We have computed internal solitary waves corresponding to different A values using density 1 with $a = 0.01$, $z_0 = 70$, and $d = 10$. Figure 4.3 gives the surface current profiles for different A values. It shows the shape of the internal solitary waves corresponding to different A . The absolute value of the extreme isopycnal displacement η_{ext} is plotted as a function of A in Figure 4.4. Also shown is the η_{ext} obtained from the conjugate flow solutions, η_{cf} . It is clear that when A increases η_{ext} increases monotonically and asymptotically approaches the conjugate flow solution. Figure 4.5 shows the variation of wave half-length λ with A . When A increases from 0.1 to 2, λ decreases. This behaviour is predicted by the KdV equation. For large A , λ increases linearly with A .

The curve of the propagation speed c as a function of A is similar to that of η_{ext} versus A . The propagation speeds of internal solitary waves reach their upper limit value of $c = 1.98289$ for $A = 50$ and subsequent larger values (Figure 4.6).

Figure 4.7 shows the relationship between η_{ext} and λ . For small amplitude waves

($\eta_{ext} < 3$), the fully nonlinear model results agree well with the KdV model results. As η_{ext} increases from about 5 to 20, the wave half-length is almost unchanged. When η_{ext} is between 20 and 20.5, increasing A causes both η_{ext} and λ to increase. When η_{ext} is greater than about 22, increasing the wave energy results in an increased wave length with insignificant change in η_{ext} .

In our calculations, the numerical resolution is $\Delta x = 12$, $\Delta z = 1$. For $A \approx 50$, the internal solitary wave propagation speed reaches its upper limit value of 1.98289 and remains constant for larger values of A . The extreme isopycnal displacements for $A = 50, 70, 100, 120$ are 22.8467, 22.8571, 22.8577 and 22.8577, respectively. It is apparent that both the extreme isopycnal displacement and wave propagation speed reach their upper limit values when $A = 100$ for internal solitary waves in this density field.

We have also calculated the extreme isopycnal displacement η_{cf} and wave propagation speed c_{cf} for the flat-centred internal solitary wave in the same density stratification (density 1) using the conjugate flow model. The accuracy used in finding the root of equation (2.46) is 10^{-6} . The results are $\eta_{cf} = 22.8616$ and $c_{cf} = 1.98274$, respectively. It is obvious that η_{ext} is bounded by and approaches asymptotically to η_{cf} as the internal solitary wave becomes flat-centred. Wave propagation speed c also approaches asymptotically to c_{cf} as A increases. The c value of a large flat-centred internal solitary wave obtained from the fully nonlinear model for $A > 50$ is about 0.0076% larger than the conjugate flow model solution. Resolution tests show

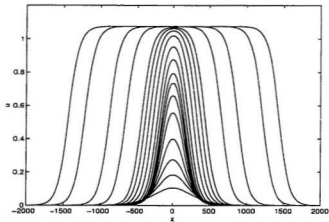


Figure 4.3: Surface current profiles for different A values. Density 1 with $\alpha = 0.01$, $z_0 = 70$ and $d = 10$. $A = 0.1, 0.25, 0.5, 1, 2, 3, 4, 5, 7, 10, 15, 20, 25, 30, 50, 70, 100, 120$.

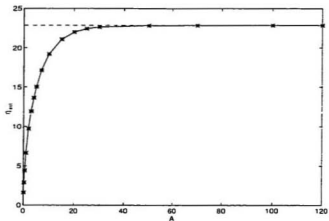


Figure 4.4: Magnitude of the extreme isopycnal displacement η_{ext} as a function of A for density 1 with $\alpha = 0.01$, $z_0 = 70$ and $d = 10$. Solid line: fully nonlinear model results; dashed line: magnitude of the extreme isopycnal displacement calculated from the conjugate flow model. Stars correspond to the values of A used.

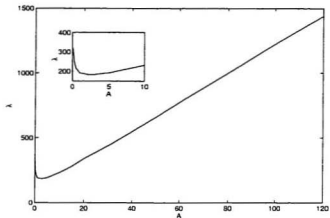


Figure 4.5: Variation of wave half-length λ with A for density 1 with $\alpha = 0.01$, $z_0 = 70$ and $d = 10$.

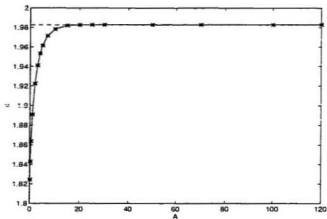


Figure 4.6: Wave propagation speed c plotted as a function of A for density 1 with $\alpha = 0.01$, $z_0 = 70$ and $d = 10$. Solid line: fully nonlinear model results, dashed line: conjugate flow model results. Stars correspond to the values of A used.

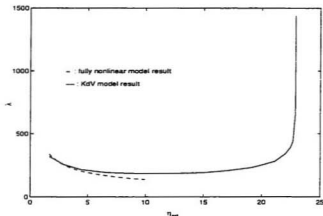


Figure 4.7: Wave half-length λ plotted as a function of the extreme isopycnal displacement η_{ext} for density 1 with $a = 0.01$, $z_0 = 70$ and $d = 10$. Dashed line: KdV model results.

that the error decreases as the numerical resolution increases, this indicates that the difference is a result of numerical error.

The vertical profiles of the horizontal velocity u at the centre of the wave for different A values are shown in Figure 4.8. The curves for $A = 50, 70, 100$ and 120 are indistinguishable from the conjugate flow solution. It reveals that the vertical profiles of u approach the conjugate flow solution as A increases. Therefore, the conjugate flow model solution describes the flow at the centre of flat-centred internal solitary waves.

We assessed the numerical simulation error caused by the left and right boundary conditions by examining the numerical results with different L values. Our results show that the results are almost not affected if the domain size ($2L$) is eight times

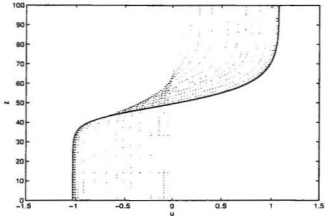


Figure 4.8: Vertical profiles of horizontal velocity u for $A = 0.1, 0.25, 0.5, 1, 2, 3, 4, 5, 7, 10, 15, 20, 25, 30, 50, 70, 100, 120$ and for conjugate flow solution. Dotted line: fully nonlinear model results; solid line: conjugate flow model solution. Dotted lines for $A = 50, 70, 100, 120$ are indistinguishable from the solid curve.

larger than the wave half-length. In our calculations, the domain is about ten times larger.

In order to check whether the internal solitary wave obtained from the fully nonlinear model will retain its shape and phase speed in propagation, we initialized a time stepping numerical model (Lamb, 1994) which solves equations (3.25)–(3.28) with a solitary wave and let it evolve for 20 hours. The reference frame moves with the phase speed of the internal solitary wave, so that the wave centre always stays at $x = 0$ if the wave propagates with constant phase speed. Figures 4.9 and 4.10 show the internal solitary waves for $A = 25$ and $A = 100$ at time $t = 0$ and $t = 20$ hours with numerical resolution $\Delta x = 10$ and $\Delta z = 1.67$. It is clear that twenty hours later the waves retain their shapes. The centres of the waves are at about $x = 50$ at $t = 20$

hours. This means the propagation speed decreases during the wave evolution. Experiments show that the error is caused by the numerical dissipation, with the error decreasing as the resolution is increased. When $\Delta x = 6.67$ and $\Delta z = 1$, the shape and position of the wave at $t = 20$ hours is almost exactly the same as at $t = 0$ with its centre stay at $x = 0$ (Figure 4.11).

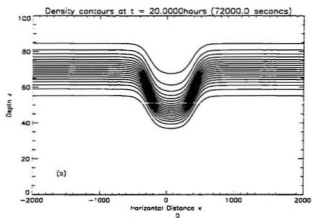
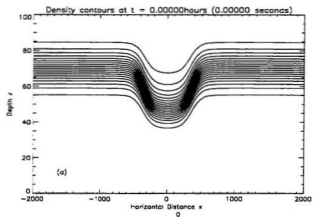


Figure 4.9: Density contours for $A = 25$ at (a) $t = 0$ and (b) $t = 20$ hours. Wave is propagating to left.

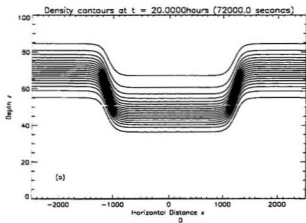
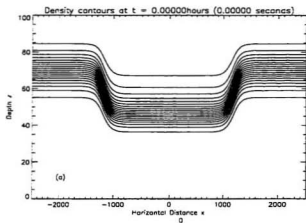


Figure 4.10: Density contours for $A = 100$ at (a) $t = 0$ and (b) $t = 20$ hours. Wave is propagating to left.

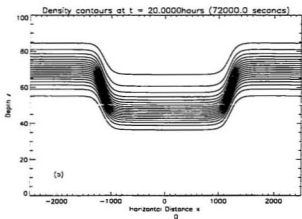
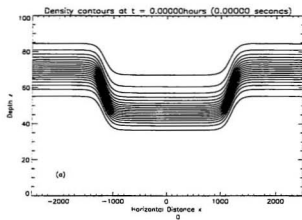


Figure 4.11: Density contours for $A = 100$ at (a) $t = 0$ and (b) $t = 20$ hours with higher numerical resolution. Wave is propagating to left.

Chapter 5

Results for Single Pycnocline Density Stratifications

Meiron and Saffman (1983) and Grimshaw and Pullin (1986) have discovered "overhanging" limiting internal periodic wave profiles at very large amplitudes. Turner and Vanden-Broeck (1988) argued that these probably arose as a consequence of their use of periodic boundary conditions in their computations and that genuine limiting internal solitary waves would tend to be very wide with a uniform flow in the middle region that is conjugate to the outskirts flow, a uniform flow far from the wave in the frame moving with the wave. It is of interest to investigate the limiting amplitudes of internal solitary waves, measured by isopycnal displacement. We showed in Chapter 4 that the conjugate flow model solution gives the upper limit of phase speed and isopycnal displacement for curves with open streamlines for stratifications in which

flat-centred waves exist provided that a conjugate flow solution exists. It may be possible to have larger waves with recirculating regions (Davis and Acrivos, 1967; Tung et al., 1982; Stamp and Jacka, 1995). The waves with recirculating regions have been observed experimentally and they are mode-2 waves (Stamp and Jacka, 1995). The properties of the conjugate flow model solutions in a single pycnocline density stratification with and without the Boussinesq approximation are investigated in this chapter.

Two density profiles are used. The first one describes a stratification with a single pycnocline centred at z_0 , given by

$$\bar{\rho}(z) = 1.0 - a \tanh\left(\frac{z - z_0}{d}\right). \quad (5.1)$$

The buoyancy frequency N is given by

$$N^2 = a \frac{g}{d\bar{\rho}(z)} \operatorname{sech}^2\left(\frac{z - z_0}{d}\right). \quad (5.2)$$

In order to examine the effects of the Boussinesq approximation, we also use the first density profile in a slightly modified form. This gives the second density profile as

$$\bar{\rho}(z) = 1.0 - 0.001d \tanh\left(\frac{z - z_0}{d}\right). \quad (5.3)$$

This density also has the hyperbolic tangent profile, and is the same as the first with

a proportional to d . For the second density stratification, N^2 is

$$N^2 = 0.001 \frac{g}{\bar{\rho}(z)} \operatorname{sech}^2\left(\frac{z - z_0}{d}\right). \quad (5.4)$$

In the limit of $d \rightarrow \infty$, $\bar{\rho}$ goes to

$$\bar{\rho}(z) = 1.0 - 0.001(z - z_0). \quad (5.5)$$

i.e., is linear in z , and N^2 goes to

$$N^2 = \frac{0.001g}{\bar{\rho}(z)}. \quad (5.6)$$

In this case the limiting buoyancy frequency is constant under the Boussinesq approximation.

5.1 Results for the First Density Stratification

We investigate the properties of the solutions for a range of d , z_0 and a values. When the Boussinesq approximation is used we need to consider only one value of a since the solutions can be scaled to obtain solutions for other a values. The reference density can be written as

$$\rho_0 = 1 - aR, \quad (5.7)$$

where R is a constant for a given density stratification and its form depends on how the reference density is chosen. We consider two options: either ρ_0 is the average of the surface and bottom density values, or it is the vertically mean density. For the first case R has the form of

$$R = \frac{\tanh\left(\frac{H-z_0}{d}\right) - \tanh\left(\frac{z_0}{d}\right)}{2}. \quad (5.8)$$

and for the second case,

$$R = \frac{1}{H} \int_0^H \tanh\left(\frac{z-z_0}{d}\right) dz. \quad (5.9)$$

In either case $\bar{\rho}(z)$ can be written as

$$\bar{\rho}(z) = (1 - aR) \left(1 - \frac{a}{1 - aR} \left(\tanh\left(\frac{z-z_0}{d}\right) - R \right) \right). \quad (5.10)$$

Since the solution of the nonlinear eigenvalue problem ($\eta(z)$, c) in (2.44) is unchanged by multiplying ρ by a constant because N^2 is unchanged, the factor $1 - aR$ can be dropped. The resulting density profile has a reference density $\rho_0 = 1$ for all values of a . Thus changing the value of a from a to \tilde{a} changes the buoyancy frequency N^2 by a factor of

$$J = \left(\frac{\tilde{a}}{1 - \tilde{a}R} \right) / \left(\frac{a}{1 - aR} \right). \quad (5.11)$$

Hence the eigenfunctions $\eta(z)$ of the eigenvalue problem are unchanged while the square of the propagation speed, c^2 , is changed by the same factor β .

When the Boussinesq approximation is not used changing a will change the eigenfunctions $\eta(z)$. Now let us examine the results of the single pycnocline density stratification for different a , z_0 and d values.

Figure 5.1 shows the variation of extreme isopycnal displacement η_{ext} as a function of z_0 for $d = 5, 10, 15$ with the Boussinesq approximation. The results show that the curves pass through 0 at $z_0 = 50$. This means that when the centre of the pycnocline is at the mid-depth $\eta(z)$ is identically 0 and there are no conjugate flow solutions. The conjugate flow solutions are elevations when the centre of the pycnocline is below the mid-depth ($z_0 < 50$) and depressions when the pycnocline is above the mid-depth ($z_0 > 50$). The absolute value of η_{ext} increases as the distance between z_0 and $H/2$ increases. This means the farther the centre of the pycnocline from the mid-depth, the larger the magnitude of η_{ext} is. The curves begin and end at the values of z_0 for which the solution is at the breaking limit which is when $\eta'(z) = 1$ first occurs. It can also be seen that the distribution of η_{ext} as a function of z_0 is antisymmetric about $z_0 = 50$. This means that the extreme isopycnal displacements η_{ext} have the same magnitude with the opposite sign when the centres of the pycnoclines are at z_0 and at $H - z_0$; one is a depression and the other an elevation. Since the density profile is antisymmetric about $z = z_0$ and the governing equations (2.1)–(2.3) with the Boussinesq approximation have a symmetric property, it is not difficult to understand

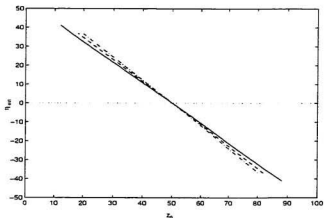


Figure 5.1: Variation of η_{ext} as a function of z_0 in the Boussinesq case for $d = 5$ (solid line), $d = 10$ (dashed line), and $d = 15$ (dash dotted line).

that the solution η_{ext} from the conjugate flow model is antisymmetric about $z_0 = 50$. If the centre of pycnocline is fixed, the magnitude of the extreme isopycnal displacement increases as d increases. As can be seen in Figure 5.1, η_{ext} is almost linear in z_0 . The slopes have magnitudes greater than one which increase linearly as d increases, being about 1.08, 1.15 and 1.22 for $d = 5, 10$ and 15 , respectively. The slope approaches 1 as $d \rightarrow 0$, i.e., in the 2-layer limit.

Figure 5.2 shows the profiles of η for $d = 10$ using the Boussinesq approximation. It is clear that the extreme isopycnal displacement happens around $z = 50$. When $z_0 > 50$, η_{ext} occurs at $z < 50$; when $z_0 < 50$, η_{ext} occurs at $z > 50$. The absolute value of η_{ext} is always greater than $|z_0 - H/2|$. This means the centre of the pycnocline is displaced past the mid-depth in the centre of the wave. For $z_0 = 70$, the extreme isopycnal displacement of -22.86 is the isopycnal which passes through $z = 49.42$ in

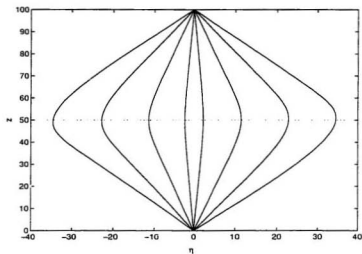


Figure 5.2: η profiles for $d = 10$ in the Boussinesq case. $z_0 = 80, 70, 60, 52, 48, 40, 30, 20$ from left to right.

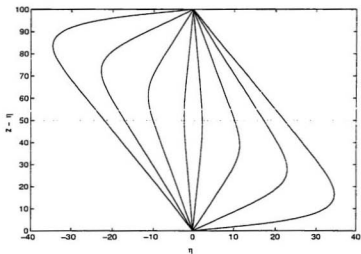


Figure 5.3: η profiles plotted as a function of $z - \eta(z)$. Same cases as in Figure 5.2. $z_0 = 80, 70, 60, 52, 48, 40, 30, 20$ from left to right.

the conjugate flow region and $z = 72.28$ in the outskirts. For a two-layer flow with the Boussinesq approximation the interface is exactly at the mid-depth in the conjugate flow region (Amick and Turner, 1986). Figure 5.3 shows the η profile as a function of $z - \eta(z)$, the height of the isopycnal in the outskirts region, for the same cases as Figure 5.2. It is clear that the isopycnal which is displaced the furthest toward the mid-depth is farther from the mid-depth than the centre of the pycnocline. When the Boussinesq approximation is not made $\eta(z)$ depends on a .

Figure 5.4 shows the variation of η_{ext} as a function of z_0 for three values of a , namely 0.01, 0.1 and 0.5 using $d = 5, 10, 15$. The solid lines are the results in the Boussinesq approximation, the dotted, dashed and dash dotted lines without the Boussinesq approximation for $a = 0.01, 0.1$ and 0.5 . As expected, as $a \rightarrow 0$ the non-Boussinesq solution approach the Boussinesq solution. Excellent agreement is obtained for $a = 0.01$, in which the lines for the Boussinesq and non-Boussinesq cases are indistinguishable. It is obvious that the difference between the results with and without the Boussinesq approximation increase as a increases; and the difference decreases as d increases. Making the Boussinesq approximation, η_{ext} is about 2.2 smaller than without the approximation for $d = 5$ and about 1.5 smaller for $d = 15$ when $a = 0.1$. If $a = 0.5$, the errors are about 11.7 for $d = 5$ and about 7.8 for $d = 15$.

Figures 5.5 and 5.6 show the density and buoyancy frequency profiles in the undisturbed and disturbed density fields for $z_0 = 80, 70, 60$, and 52 . In the disturbed

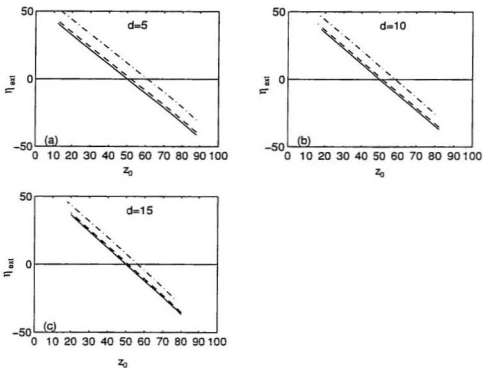


Figure 5.4: η_{ext} for conjugate flow solution plotted as a function of z_0 for $a = 0.01$ (dotted line), $a = 0.1$ (dashed line) and $a = 0.5$ (dash dotted line) in the non-Boussinesq case. Solid lines are the Boussinesq approximation results. (a) $d = 5$. (b) $d = 10$. (c) $d = 15$.

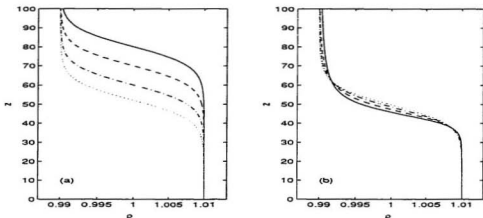


Figure 5.5: Density profiles in (a) undisturbed and (b) disturbed density fields with the Boussinesq approximation for $a = 0.01$, $d = 10$, $z_0 = 80$ (solid line), 70 (dashed line), 60 (dash dotted line), 52 (dotted line).

region, the pycnocline is near the mid-depth; the maximum buoyancy frequency decreases as z_0 approaches $H/2$.

We now turn to the propagation speed c . When the Boussinesq approximation is applied c depends on both a and the reference density ρ_0 (as both a and ρ_0 change $N^2(z)$ by a constant multiple). We first choose the average of bottom and surface densities as the reference density ρ_0 . Figure 5.7 shows the distribution of phase speed c as a function of z_0 for $a = 0.01$ and $d = 5, 10$ and 15 with and without the Boussinesq approximation. The Boussinesq results are indistinguishable with the non-Boussinesq results for $a = 0.01$. With the Boussinesq approximation, the largest phase speed occurs at $z_0 = 50$ and the amplitude of the wave is zero for this value of z_0 ; the phase speed c is smaller for a thicker pycnocline (larger d) than for a thinner

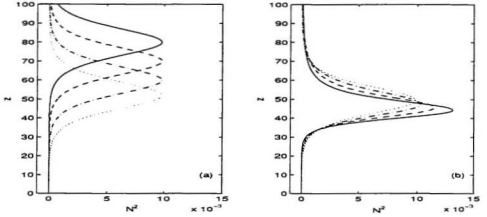


Figure 5.6: Same cases as Figure 5.5 for N^2 profiles.

pycnocline (smaller d) because N^2 increases as d decreases. Unlike the magnitude of η_{ext} , the phase speed c is not symmetric about $z_0 = 50$, because the reference densities for $z_0 = q$ and $z_0 = H - q$ are different. When $z_0 = q$, where q is a constant, the reference density is

$$\rho_{01} = 1 - a \frac{\tanh \frac{H-q}{d} - \tanh \frac{q}{d}}{2}. \quad (5.12)$$

When $z_0 = H - q$, the reference density is

$$\rho_{02} = 1 - a \frac{\tanh(\frac{q}{d}) - \tanh(\frac{H-q}{d})}{2} = 1 + a \frac{\tanh(\frac{H-q}{d}) - \tanh(\frac{q}{d})}{2}. \quad (5.13)$$

In general it is apparent that the reference densities $\rho_{01} \neq \rho_{02}$. Thus, the N^2 for z_0 and N^2 for $H - z_0$ are not symmetric about $z_0 = 50$. Figures 5.8 and 5.9 show variations of phase speed c as a function of z_0 for $a = 0.1$ and $a = 0.5$, respectively.

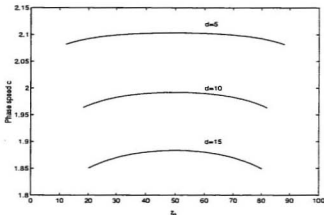


Figure 5.7: Variation of phase speed c as a function of z_0 for $a = 0.01$ and $d = 5, 10, 15$ in the Boussinesq (solid line) and non-Boussinesq (dashed line) cases. The latter are indistinguishable from the former at this scale.

Comparing the c values for $a = 0.01$ and $a = 0.5$ confirms that c^2 increases by a factor of \mathcal{J} given by (5.11) in the Boussinesq approximation. For $a = 0.1$, the errors in c caused by the Boussinesq approximation are 0.0083 for $d = 5$ and 0.0070 for $d = 15$. For $a = 0.5$, the errors in c caused by the Boussinesq approximation are 0.5147 for $d = 5$ and 0.4423 for $d = 15$. The relative difference in c is about 0.12% for $a = 0.1$ and about 3.34% for $a = 0.5$.

We also examine the case in which the reference density used for the Boussinesq approximation is taken as the vertical mean of the density in order to determine the effect of the choice of the reference density on the phase speed. Since the variation of the reference density will only affect the buoyancy frequency, the solution of $\eta(z)$ will be the same as when the reference density is the average of the bottom and surface

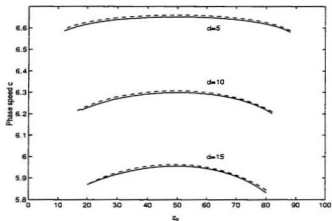


Figure 5.8: Phase speed c plotted as a function of z_0 for $a = 0.1$. Solid line: with the Boussinesq approximation; dashed line: without the Boussinesq approximation.

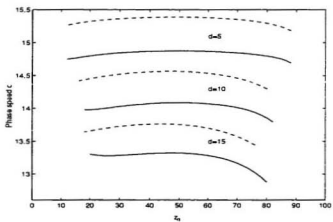


Figure 5.9: Same as Figure 5.8 for $a = 0.5$.

densities. The phase speed c will change. Figure 5.10 shows the phase speed c as a function of z_0 for $a = 0.01, 0.1, 0.5$ with $d = 10$ in the cases with and without the Boussinesq approximation. It is clear that the Boussinesq approximation using the average of surface and bottom densities as the reference density results in smaller errors for all the three a values than that using the vertically mean density. The use of the vertically mean density results in significant differences in the propagation speed for this density stratification. In the remainder of the thesis, we use the average of the surface and bottom densities as the reference density without further investigation.

The horizontal velocity profiles $U(z)$ are shown in Figure 5.11 for different z_0 values using $d = 10$ with the Boussinesq approximation. When $z_0 = 50$, the maximum density stratification is at the mid-depth, there are no conjugate flow solutions and $U(z) = 0$. If z_0 moves away from $z_0 = 50$, the magnitudes of horizontal velocities at both bottom and surface boundaries increase. At the layers near the surface and bottom boundaries, the fluid velocities are almost constant. This is because the density near the boundaries is almost constant, thus the flow is irrotational, i.e., $U_z - w_x \approx 0$. Since the boundaries are rigid-lid, no vertical flow at the boundaries, $w = 0$, so that $U_z \approx 0$. U is nearly constant near the boundaries.

The valid conjugate flow solutions can be obtained only for a range of z_0 values which satisfy $z_l(d) < z_0 < z_u(d)$. $z_l(d)$ and $z_u(d)$ are the lower and upper breaking limit of z_0 values in which $\eta'(z) = 1$ first occurs. In Figure 5.12 the breaking curves $z_0 = z_l(d)$ and $z_0 = z_u(d)$ and contours of the minimum Richardson numbers for

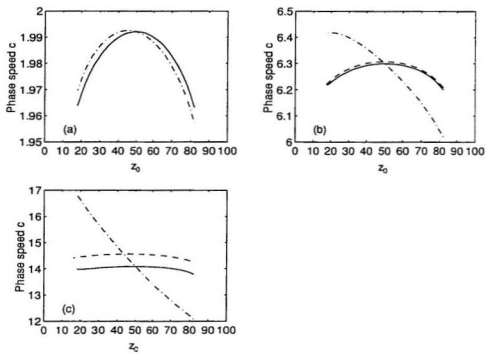


Figure 5.10: Comparison of phase speed c as a function of z_0 for $d = 10$. (a) $a = 0.01$. (b) $a = 0.1$. (c) $a = 0.5$. Curves are for the non-Boussinesq case (dashed line), the Boussinesq case with the average value of the surface and bottom densities as the reference density (solid line) and with the vertically mean density as the reference density (dash dotted line).

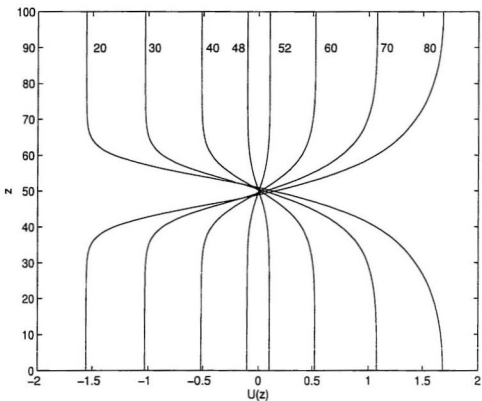


Figure 5.11: Horizontal velocity $u(z)$ profile at the centre of flat-centred internal solitary wave for $a = 0.01$, $d = 10$ with the Boussinesq approximation. $z_0 = 20, 30, 40, 48, 52, 60, 70, 80$ from left to right in the upper half.

$Ri = 0.25, 0.5, 1.0$ are shown for the Boussinesq case (for which the curves are independent of a) and for the non-Boussinesq cases with $a = 0.01$ and $a = 0.1$. The Richardson number is defined as

$$Ri(z) = \frac{N^2}{L_z^2}, \quad (5.14)$$

where N^2 is the square of buoyancy frequency and L_z is the gradient of horizontal velocity $U(z)$ in the conjugate flow region. It needs to be pointed out that

$$N^2 = -\frac{g}{\bar{\rho}_p(z)} \bar{\rho}'_p(z) = -\frac{g}{\bar{\rho}(z-\eta)} \frac{d\bar{\rho}}{dz} (z-\eta)(1-\eta'). \quad (5.15)$$

The linear stability condition is

$$Ri > 0.25 \quad (5.16)$$

everywhere in the flow (Kundu, 1990). $Ri < 0.25$ is a necessary but not sufficient condition for instability. Figure 5.12 indicates that there are no conjugate flow solutions if d and z_0 lie outside the two breaking limits. This occurs when the centre of the pycnocline gets too close to the upper or lower boundary. It should be emphasized that although there are no conjugate flow solutions, solitary waves are still possible. For these stratifications as the wave amplitude increases the solitary waves break before a limiting, flat-centred wave is formed. The conjugate flow is linearly stable if d and z_0 are between the two $Ri = 0.25$ contours and potentially unstable

if d and z_0 are in between the breaking limit and $Ri = 0.25$ contour. The region of potentially unstable flow increases as d decreases below about 8.4. As $d \rightarrow 0$, $z_i \rightarrow 0$, $z_u \rightarrow H$ and the contour of $Ri = 0.25$ tend to meet at $z_0 = 50$. the minimum Ri number is below 0.25 for all z_0 , so that the flow is potentially unstable for all values of z_0 . In the two-layer limit, there is a velocity jump across the interface, thus the fluid is always unstable for sufficiently small horizontal wavelengths (Kundu, 1990). When the Boussinesq approximation is applied, the breaking limit curves and the minimum Ri number contours are symmetric about $z_0 = 50$. In addition, because changing a leaves N^2/c^2 and $\eta(z)$ unchanged, the breaking curve and the Richardson number are independent of a . It is clear that the results in the Boussinesq case are almost identical to the non-Boussinesq case for $a = 0.01$; for $a = 0.1$ the non-Boussinesq effect is large. In the non-Boussinesq case, the breaking limit curves are moved down slightly by an amount that increases approximately linearly with d from a negligible amount for small values of d to about 1.1 at $d = 30$. The curves of $Ri = 0.25, 0.5, 1.0$ are moved up about 2.4 at $d = 1.0$; the difference decreases as d increases until the two lines (solid line and dotted line) intersect, then the difference increases as d increases.

The above comparisons of the solutions obtained with and without the Boussinesq approximation suggest that for $a = 0.01$, the Boussinesq approximation is very good. For this value of a there is a 2% change in density between the surface and the bottom. When $a = 0.1$, which represents a 20% density change from surface to bottom, the errors caused by the Boussinesq approximation are large. In the real

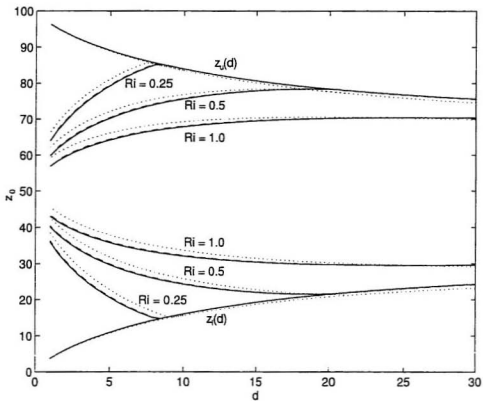


Figure 5.12: The breaking curves $z_l(d)$ and $z_u(d)$ and contours of minimum Richardson number for density 1. Curves are for Boussinesq case (solid) and non-Boussinesq cases for $\alpha = 0.01$ (dashed) and $\alpha = 0.1$ (dots).

ocean, the density variation from surface to bottom is usually less than 1%, so that the Boussinesq approximation is appropriate for the oceanographic conditions if there is a well defined pycnocline (e.g., with d less than 20% of the fluid depth). As discussed in the next section, the Boussinesq approximation gives large errors if the density profile is nearly linear, or if d is comparable to the half fluid depth.

5.2 Results for the Second Density Profile

We compare the results of the conjugate flow model solutions for the second density profile given by (5.3) with and without the Boussinesq approximation and analyze the validity of the Boussinesq approximation in this density stratification. Figure 5.13 shows the density and buoyancy frequency profiles for $d = 10, 100, 1000$ and $z_0 = 70$. The dashed line in Figure 5.13b is N^2 using the Boussinesq approximation with the reference density $\rho_0 = 1$. As $d \rightarrow \infty$, the density field becomes linear and N^2 is constant ga/ρ_0 in the Boussinesq approximation and the curve of N^2 is a hyperbola without the Boussinesq approximation. Under the Boussinesq approximation N^2 is a constant, the eigenvalue problem linearizes and has an infinite number of solutions

$$\eta(z) = A_m \sin\left(\frac{\pi}{H}z\right) \quad (5.17)$$

where the amplitude A_m is an arbitrary constant. If the Boussinesq approximation is not made, then N^2 increases monotonically with z in the limit $d \rightarrow \infty$. There is no

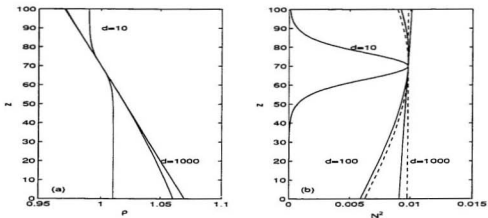


Figure 5.13: Density (a) and N^2 (b) profiles for $z_0 = 70$ and $d = 10, 100, 1000$. In (b), the dashed line and solid line are with and without the Boussinesq approximation, respectively.

solution for the eigenvalue problem. This indicates that the Boussinesq approximation is not valid because it leads to serious errors. We need to know for what value of d the Boussinesq approximation is valid in this density field.

Figures 5.14 and 5.15 shows the variation of η_{ext} , c , $\eta'(0)$ and $\eta'(H)$ as a function of d for the density field with the centre of the pycnocline at $z_0 = 60$ and $z_0 = 70$. $\eta'(0)$ and $\eta'(H)$ are the derivative of $\eta(z)$ with respect to z at $z = 0$ and $z = H$, respectively. For $z_0 = 60$, it is clear that the results in the cases with and without the Boussinesq approximation agree well only for $d < 35$. As d increases above 35 the difference increases. When the Boussinesq approximation is not made, the solution breaks down ($\eta'(H) = 1$) when $d > 170$. The Boussinesq solution asymptotes to a solution with $\eta_{ext} \approx -15$, $\eta'(0) \approx -0.46$, $\eta'(H) \approx 0.46$. The absolute values are

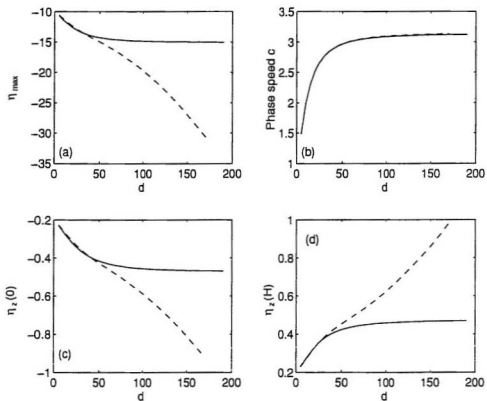


Figure 5.14: η_{ext} (a), c (b), $\eta'(0)$ (c), and $\eta'(H)$ (d) versus d for $z_0 = 60$ in the second density field for the Boussinesq (solid line) and non-Boussinesq (dashed line) cases.

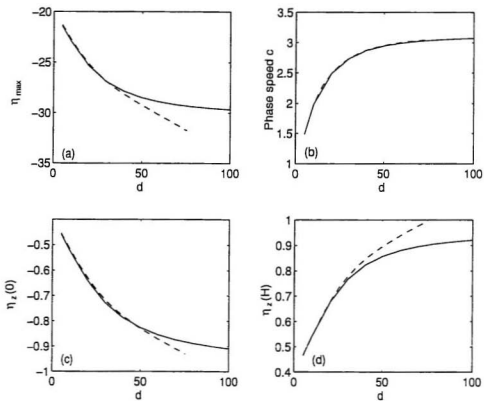


Figure 5.15: η_{ext} (a), c (b), $\eta'(0)$ (c), and $\eta'(H)$ (d) versus d for $z_0 = 70$ in the second density field for the Boussinesq (solid line) and non-Boussinesq (dashed line) cases.

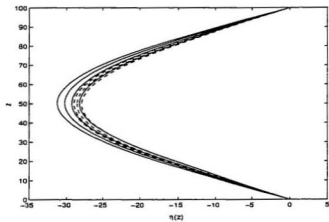


Figure 5.16: $\eta(z)$ profiles for $z_0 = 70$. $d = 70, 60, 50, 40$ from left to right. Solid lines: non-Boussinesq case; dashed lines: Boussinesq case.

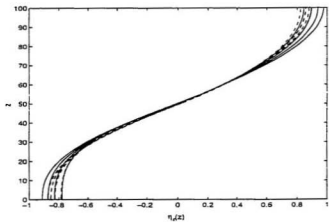


Figure 5.17: $\eta_z(z)$ profiles for $z_0 = 70$. $d = 40, 50, 60, 70$ from left to right in the upper part. Solid lines: non-Boussinesq case; dashed lines: Boussinesq case.

much smaller than those of $\eta_{ext} \approx -30$, $\eta'(0) \approx -0.93$, $\eta'(H) = 1.0$ at the breaking point for the non-Boussinesq solution. Similar behaviour is seen for other values of z_0 . As z_0 increases the non-Boussinesq solution breaks at smaller d values and the asymptotic limits of η_{ext} , $\eta'(0)$, $\eta'(H)$ for the Boussinesq solution increases in magnitude (Figure 5.15).

Figures 5.16 and 5.17 are the profiles of the isopycnal displacement $\eta(z)$ and $\eta'(z)$ of the internal solitary wave in the density field with $z_0 = 70$ for $d = 40, 50, 60$ and 70 . The solid lines are the results without the Boussinesq approximation and dashed lines with the approximation. It also shows that the errors of $\eta(z)$ and $\eta'(z)$ in the Boussinesq approximation increases as d increases. The above analysis confirms the argument that the Boussinesq approximation may lead to serious errors for some stratifications.

Chapter 6

Results for Density Stratifications with Two Pycnoclines

In this chapter, we consider density stratifications with two pycnoclines centred at height z_1 and z_2 with thickness d_1 and d_2 , respectively. The density (we called density 2 hereafter) in the undisturbed region is

$$\bar{\rho}(z) = 1 - a_1 \tanh\left(\frac{z - z_1}{d_1}\right) - a_2 \tanh\left(\frac{z - z_2}{d_2}\right). \quad (6.1)$$

a_1 and a_2 are parameters measuring the strength of the stratifications. For a stable stratification, a_1 and a_2 are both positive. When the two pycnoclines are well separated and away from the boundaries, the density decreases by $2a_1$ and $2a_2$ across the two pycnoclines. We present the results of the conjugate flow model for this density

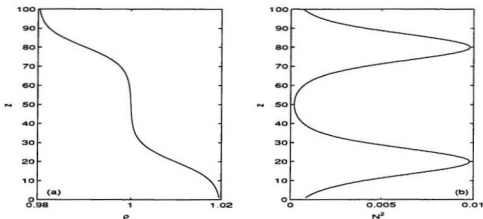


Figure 6.1: Density $\bar{\rho}$ (a) and N^2 (b) profiles for density 2 with $a_1 = a_2 = 0.01$, $d_1 = d_2 = 10$, $z_1 = 20$, $z_2 = 80$ with the Boussinesq approximation.

stratification for the parameters a_1 , a_2 , z_1 , z_2 , d_1 and d_2 with a range of values in the cases with and without the Boussinesq approximation.

6.1 Case 1: $a_1 = a_2 = a$, $d_1 = d_2 = d$, $z_2 = H - z_1$

In this case, the two pycnoclines are the same distance from the mid-depth and the density $\bar{\rho}(z)$ is antisymmetric about the mid-depth. When the Boussinesq approximation is made, N^2 is symmetric about the mid-depth. Figure 6.1 shows the density and N^2 profiles for this density stratification with $a = 0.01$, $d = 10$ and $z_1 = 20$ in the Boussinesq case.

Figure 6.2 is the variation of η_{ext} as a function of z_1 with and without the Boussinesq approximation. The curves are symmetric about $z_1 = 50$.

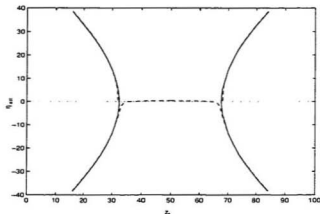


Figure 6.2: Variation of η_{ext} as a function of z_1 for density 2 with $a_1 = a_2 = 0.01$, $d_1 = d_2 = 10$, $z_2 = H - z_1$. Solid line: Boussinesq approximation; dashed line: without the Boussinesq approximation.

In the Boussinesq case, the curves are also symmetric about z_1 axis. When $z_1 = 50$, the centres of the two pycnoclines overlap and the stratification becomes the single pycnocline case with the centre of the pycnocline at the mid-depth, so that there is no conjugate flow solution. The single pycnocline stratification is a special case of the two-pycnocline stratification. Corresponding to each value of z_1 , there are either two solutions (2 η_{ext} values) or no solutions ($\eta_{ext} = 0$). When z_1 (also z_2) is close to the mid-depth ($32.44 < z_1 < 67.56$), there are no non-zero solutions. This result shows that no flat-centred waves exist. When the centres of the pycnoclines are close to the boundaries ($z_1 < 14$ or $z_1 > 86$), the conjugate flow breaks down. When $16 < z_1 < 32.44$ or $67.56 < z_1 < 84$, there are two solutions for each value of z_1 . One solution is an elevation and the other is a depression.

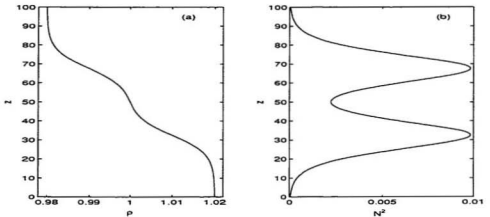


Figure 6.3: Density (a) and N^2 (b) profiles in undisturbed (solid line) and disturbed (dashed line) regions for density 2 with $a_1 = a_2 = 0.01$, $d_1 = d_2 = 10$ and $z_1 = 32.44$ ($z_2 = H - z_1$).

When the Boussinesq approximation is not made N^2 is no longer symmetric about $z = 50$. An odd number of solutions can now exist. For $z_1 = 50$ there is a single pycnocline centred at the mid-depth as shown in section 5.1, the solution is a small elevation. As z_1 decreases a single small elevation is found until $z_1 \approx 37$. For smaller values of z_1 a single small depression is obtained until at $z_1 \approx 32$, the solution bifurcates. And two solutions, an elevation and a depression are obtained.

Figure 6.3 shows the density and N^2 profiles in the disturbed and undisturbed regions for $a = 0.01$, $z_1 = 32.44$ and $d = 10$ in the Boussinesq case. In this case there is no conjugate flow solutions, so that the disturbed profile is identical with the undisturbed profile.

In Figure 6.4, the curve of propagation speed as a function of z_1 is symmetric

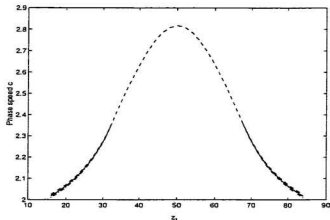


Figure 6.4: Propagation speed c plotted as a function of z_1 . Same cases as in Figure 6.2. Curves are for Boussinesq case (solid line) and non-Boussinesq case for depressed wave (dashed line) and elevated wave (dash dotted line).

about $z_1 = 50$ for both the Boussinesq and non-Boussinesq cases. The propagation speed increases as z_1 approaches the mid-depth. In the non-Boussinesq case, the propagation speeds of the depression is slightly larger than that of the elevation.

6.2 Case 2: $a_1 = a_2 = a$, $d_1 = d_2 = d$, $z_2 \neq H - z_1$

In this case the N^2 profile is no longer symmetric about the mid-depth. We will discuss the most significant findings for various values of a , d , z_1 and z_2 . Figure 6.5 shows the variation of the extreme isopycnal displacement as a function of z_1 for various values of z_2 using $d = 10$. The results with the Boussinesq approximation are plotted in solid lines and without the Boussinesq approximation with $a = 0.01$

in dashed lines and $a = 0.1$ in dash dotted lines. The most striking feature of the results is the occurrence of multiple solution branches.

The solutions with the Boussinesq approximation are discussed first. For $z_2 = 50$, three solution branches are found. The main branch occurs in the range with z_1 between about 14 and 86. The other two branches occur in a range with z_1 close to the boundaries, one is for $z_1 < 8.5$ and the other for $z_1 > 91.5$. When $z_1 = 50$, the two pycnoclines overlap to form a single pycnocline with its centre at the mid-depth. There is no conjugate flow solution. This is in agreement with the single pycnocline case. The main solution branch shows an elevation for $z_1 < 50$ and a depression for $z_1 > 50$. This is the same feature as that of the single pycnocline case: when the centre of the pycnocline is in the upper/lower half of the fluid layer, the conjugate flow solutions are depressed/elevated. As z_1 moves further away from the mid-depth, the magnitude of the extreme isopycnal displacement increases until the breaking solution is reached at about $z_1 = 12$ and 88. There is no solution for z_1 between about 8.5 and 12 and between about 88 and 91.5. When z_1 is close to the boundaries, two solutions are obtained again. For $z_2 = 50$ the two solutions are elevations for $z_1 < 8.5$ and depressions for $z_1 > 91.5$. The solutions are antisymmetric about $z_1 = 50$.

As z_2 increases the forms of the three solution branches change. The zero point of the main branch moves to the left. For z_2 between 50 and about 67.6 the zero point is at $H - z_2$. For this value of z_1 the buoyancy frequency is symmetric about the mid-depth, there is no conjugate flow solution as discussed in the previous section.

The left solution branch increases and the right solution branch decreases in size and they both move downward as z_2 increases. When $z_2 = 60$, the right solution branch disappears and the main and the left branches overlap, so that there are three solutions for some values of z_1 . The region of overlap increases as z_2 increases. The two branches join and form corners at z_2 between 67.6 and 67.7 (Figure 6.6). For larger values of z_2 there are again two solution branches. One branch is a depression over a large range (from 0 to about 86) of z_1 values (called the main branch) and the other branch (upper branch) has two solutions for some values of z_1 . Thus three solutions are obtained for some values of z_1 . For $z_2 > 67.56$, there are two solutions for $z_1 = H - z_2$, one is an elevation and the other is a depression. This is the case discussed previously in section 6.1. Along the upper branch $\eta_{ext} = 0$ at $z_1 = H - z_2$ for $z_2 > 67.56$. The elevation and depression have the same propagation speed and the same extreme isopycnal displacement in magnitude. For example, for $z_2 = 80$ and $z_1 = 20$, $\eta_{ext} = 32.7402$ and $c = 2.064807$ for the elevation and $\eta_{ext} = -32.7402$ and $c = 2.064807$ for the depression. The lower part of the upper branch crosses z_1 axis at $z_1 = 20$ (Figure 6.5g). The main solution branch flattens and the region of the upper solution branch increases as z_2 increases.

The solutions for the non-Boussinesq case with $a = 0.01$ are very similar to the Boussinesq solutions. The largest difference occurs near the point where the two-solution branches join near $z_2 = 67.7$ (Figure 6.6). For $z_2 = 67.6$, the Boussinesq solution has the left and right branches, while the non-Boussinesq solution has upper

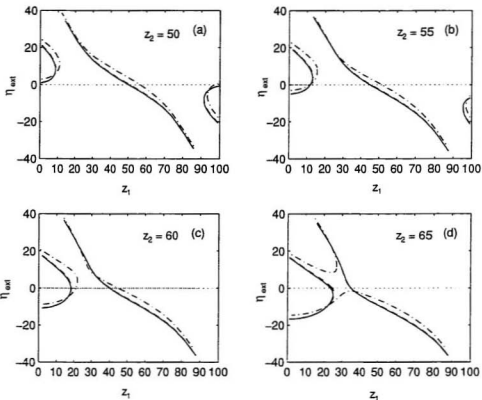


Figure 6.5: Variations of η_{ext} as a function of z_1 for density 2 for various values of z_2 . $\alpha_1 = \alpha_2 = a$ and $d_1 = d_2 = 10$. Solutions for the Boussinesq case (solid line) and non-Boussinesq cases for $a = 0.01$ (dashed line) and $a = 0.1$ (dash dotted line) are shown.

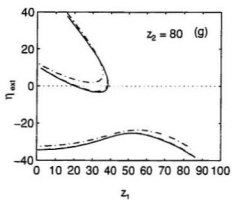
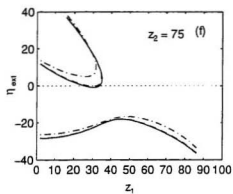
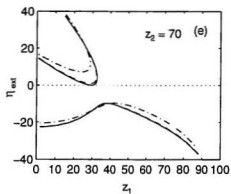


Figure 6.5: Continued

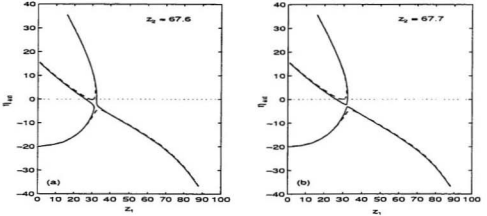


Figure 6.6: Joining of solution branches for density 2 when η_{ext} is plotted as a function of z_1 . $a_1 = a_2$, $d_1 = d_2 = 10$. Boussinesq case (solid line) and non-Boussinesq case for $a = 0.01$ (dashed line). (a) $z_2 = 67.6$; (b) $z_2 = 67.7$.

and lower branches. When $a = 0.01$, there is approximately a 4% change in density from surface to bottom. This is extremely large for coastal ocean regions. When a increases to 0.1, the differences between the Boussinesq and non-Boussinesq solutions increase. For example, when $z_2 = 50$ the left solution branch extends further to the right by about 2.4 in z_1 value and the right solution branch shrinks by a similar amount. The form of the solution changes from left and right branches to upper and lower branches for z_2 is between 60 and 65. When $z_2 = 80$, the upper branch in the non-Boussinesq case is always above the z_1 axis.

Figure 6.7 shows the propagation speed c as a function of z_1 for density 2 with the Boussinesq approximation for different z_2 values. The propagation speed c increases as z_1 moves closer to z_2 and the largest c value occurs near $z_1 = z_2$. For $z_2 > 67.56$,

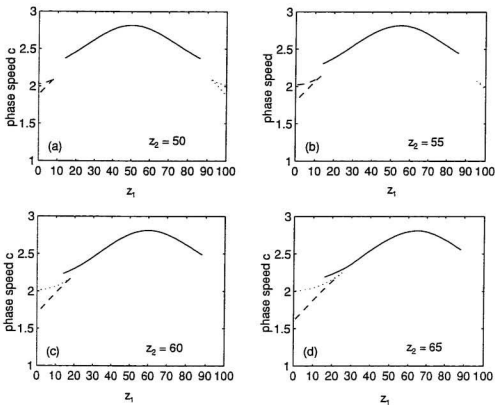


Figure 6.7: Propagation speed c as a function of z_1 for density 2 with the Boussinesq approximation. $a_1 = a_2 = a$. $d_1 = d_2 = 10$. Solid lines correspond to the main solution branches. For $z_2 = 60.65$, the dashed/dotted lines correspond to the upper/lower part of the left solution branch. For $z_2 = 70.75, 80$, the dashed/dotted lines correspond to the upper/lower part of the upper solution branch.

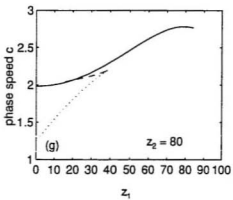
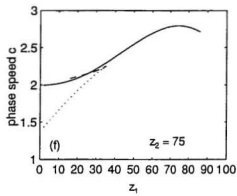
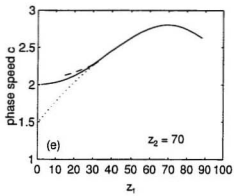


Figure 6.7: Continued

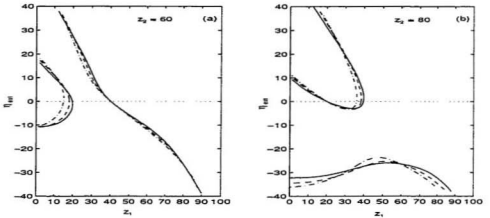


Figure 6.8: Dependence of η_{ext} on d for density 2 in the Boussinesq case. Plotted as a function of z_1 for $z_2 = 60$ (a) and $z_2 = 80$ (b). $a_1 = a_2 = 0.01$, $d_1 = d_2 = 5$ (solid line), 10 (dashed line) and 15 (dash dotted line).

the elevation and depression propagate at the same speed c when $z_1 = H - z_2$. This is shown in panels (e), (f) and (g) in Figure 6.7 where the dashed line crosses the solid line at point $z_1 = H - z_2$.

The dependence of η_{ext} on d for $z_2 = 60$ and 80 in the Boussinesq case are presented in Figure 6.8. As d increases the right limits of the left branch for $z_2 = 60$ and the upper branch for $z_2 = 80$ decrease and the region in which the three solutions exist decreases significantly.

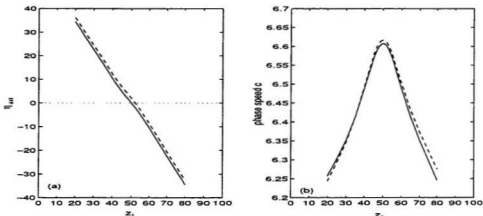


Figure 6.9: Variation of η_{ext} (a) and propagation speed c (b) as a function of z_1 for density 2 with $d_1 = d_2 = 10$, $a_1 = 0.1$, $a_2 = 0.01$, $z_2 = H - z_1$. Solid line: Boussinesq case; dashed line: non-Boussinesq case.

6.3 Case 3: $a_1 \neq a_2$, $d_1 = d_2 = d$

In Figure 6.9 the variation of η_{ext} and propagation speed c are plotted as a function of z_1 for density 2 with $d_1 = d_2 = 10$, $a_1 = 0.1$, $a_2 = 0.01$ for the case when $z_2 = H - z_1$, i.e., the two pycnoclines are equidistant from the mid-depth. The pycnocline centred at z_1 is ten times stronger than the one centred at z_2 . The results are much like the case of single pycnocline centred at z_1 (Figure 5.4b) and have the properties of the single pycnocline case. In the Boussinesq case, there is no solution when $z_1 = 50$ and solution is an elevation/depression when the centre of the strong pycnocline (z_1) is in the lower/upper half of the fluid layer. The strong pycnocline dominates the behaviour. There is no multiple solution in this case.

Figure 6.10 shows the solutions as a function of z_1 with z_2 fixed for density 2

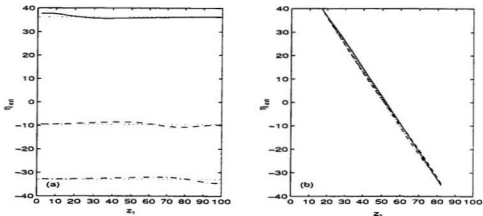


Figure 6.10: η_{zt} plotted as a function of z_1 for density 2 with $d = 10$ in the non-Boussinesq case for $z_2 = 20$ (solid line), 60 (dashed line), 80 (dash dotted line). Dotted line is the result when only the stronger pycnocline presents. (a) $a_1 = 0.01, a_2 = 0.1$; (b) $a_1 = 0.1, a_2 = 0.01$.

with $d_1 = d_2 = 10$ in the non-Boussinesq case. In panel (a) solutions with $a_1 = 0.01$ and $a_2 = 0.1$ are shown for $z_2 = 20, 60, 80$. The variation of η_{zt} is small in the whole region of z_1 . If only the stronger pycnocline were present the solution would be independent of z_1 and would be given straight lines with values of about 36.3, -9.5, and -32.8 for $z_2 = 20, 60, 80$, respectively (dotted lines in Figure 6.10a). The presence of the second weaker pycnocline whose position depends on z_1 results in small variations about these straight lines. Similar conclusions can be made from panel (b). Since the pycnocline centred at z_1 is ten times stronger than the other one, the results are much like the case in which only the pycnocline centred at z_1 exists. The variation of the centre of the weaker pycnocline has little influence on the results.

Figure 6.11 shows the variation of propagation speed c versus z_1 for the same

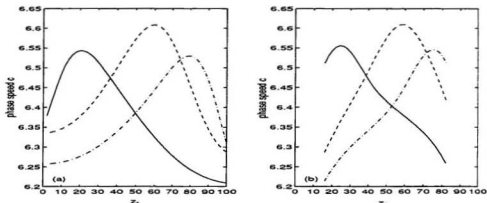


Figure 6.11: Propagation speed c versus z_1 for density 2 with $d = 10$ in the non-Boussinesq case for $z_2 = 20$ (solid line), 60 (dashed line), 80 (dash dotted line). (a) $a_1 = 0.01, a_2 = 0.1$; (b) $a_1 = 0.1, a_2 = 0.01$.

cases as in Figure 6.10. The maximum propagation speed occurs at different place compared to the single pycnocline case (Figure 5.10(b)). In the single pycnocline case, the maximum phase speed occurs when z_0 approaches the mid-depth. In the case with the stronger pycnocline centred at z_2 , the maximum phase speed occurs when z_1 is near z_2 (Figure 6.11a). If the stronger pycnocline is centred at z_1 , the maximum phase speed again occurs when z_1 is near z_2 , but in this case its position is shifted towards the mid-depth. In all cases the propagation speed is within 5% change of the value for a single pycnocline with $a = 0.1$.

In figure 6.12 the extreme isopycnal displacement η_{ext} is plotted as a function of z_1 for density 2 when the largest density gradient of one pycnocline is double that of the other for $z_2 = 60$ and 80. The dotted line represents the result when only

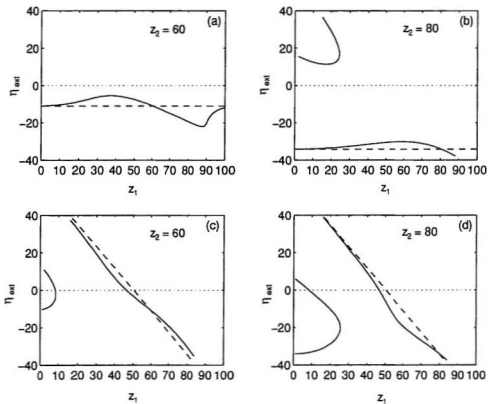


Figure 6.12: Variation of η_{ext} as a function of z_1 for density 2 when the largest density gradient of one pycnocline is double that of the other for $z_2 = 60$ and 80 in the non-Boussinesq case (solid lines). Panels (a), (b): $a_1 = 0.01$, $a_2 = 0.02$; panels (c), (d): $a_1 = 0.02$, $a_2 = 0.01$. The dashed lines are the results when only the stronger pycnocline exists.

the stronger pycnocline exists. It is clear that the stronger pycnocline dominates the behaviour and the weaker pycnocline only results in a small variation. The difference from the single pycnocline results is that the multiple solutions exist for some z_1 values. From the above analysis we suggest that the multiple solutions occur only when the strengths of the two pycnocline are comparable. When one pycnocline is much stronger than the other, the result is much like the one pycnocline case and only one solution exists.

6.4 Case 4: $a_1 = a_2 = 0.01$, $d_1 \neq d_2$, $z_1 \neq H - z_2$

Figure 6.13 shows solutions without the Boussinesq approximation for $a_1 = a_2 = 0.01$ and $d_1 \neq d_2$ for $z_2 = 60$. For comparison, the results with $d_1 = d_2$ are also shown. Panels (a), (c) and (e) show solutions with d_1 fixed and $d_2 = 5$ (solid line), 10 (dashed line) and 15 (dash dotted line) and panels (b), (d) and (f) are solutions with d_2 fixed and $d_1 = 5$ (solid line), 10 (dashed line) and 15 (dash dotted line). When d_1 is fixed at 15 and 10, the solutions change from a form with left and right (main) branches to a form with upper and lower (main) branches as d_2 decreases. The two branches join at a value of d_2 between 15 and 10 for $d_1 = 15$ and d_2 between 10 and 5 for $d_1 = 10$. When d_1 is fixed at 5, the solution has left and right branches with the left branch decreasing as d_2 increases. Upper and lower branches form for sufficiently small d_2 . The lower (main) branch of the solution for $d_1 = 15$ and $d_2 = 5$ is much

like the case of single pycnocline centred at z_2 except for the upper branch. The curve would be independent of z_1 and would be a straight line with a value of close to -10 if only the pycnocline centred at z_2 with $d_2 = 5$ were given. Panels (b), (d) and (f) show the results when d_2 is fixed. It is clear from the figures that the thinner pycnocline has a stronger influence on the solution than does the thicker one. This is because the thinner pycnocline has the largest buoyancy frequency. Figure 6.14 shows the variation of η_{ext} as a function of z_1 in the same cases as in Figure 6.13 but for $z_2 = 80$. The solutions have upper and lower (main) branches except for the case of $d_1 = 5$ and $d_2 = 15$, where the solution has left and right branches. When d_1 is fixed, the upper branch shrinks and the lower branch flattens as d_2 decreases: when d_2 is fixed, the upper branch shrinks and the lower branch flattens as d_2 increases.

6.5 Internal Solitary Waves Corresponding to Conjugate Flow Solutions

When N^2 is symmetric about the mid-depth, the flat-centred internal solitary waves corresponding to the two conjugate flow solutions can easily be obtained if the conjugate flow solutions exist. One is a wave of elevation and the other is a wave of depression with the same amplitude in magnitude and the same propagation speed. When N^2 is not symmetric about the mid-depth, there are three conjugate flow solutions for some values of z_1 . Now let us see whether each solution corresponds to

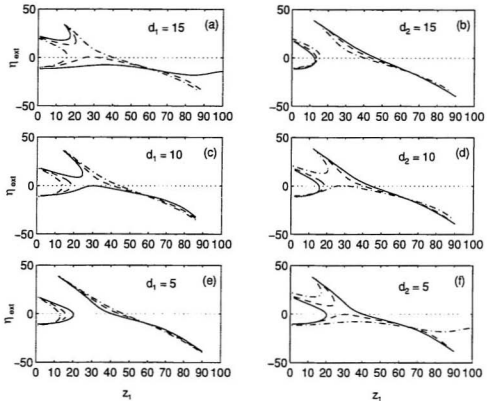


Figure 6.13: Variation of η_{ext} as a function of z_1 for density 2 with $a_1 = a_2 = 0.01$ and $z_2 = 60$ without the Boussinesq approximation. Panels (a), (c), (e): d_1 fixed and $d_2 = 5$ (solid line), 10 (dashed line) and 15 (dash dotted line); panels (b), (d), (f): d_2 fixed and $d_1 = 5$ (solid line), 10 (dashed line) and 15 (dash dotted line).

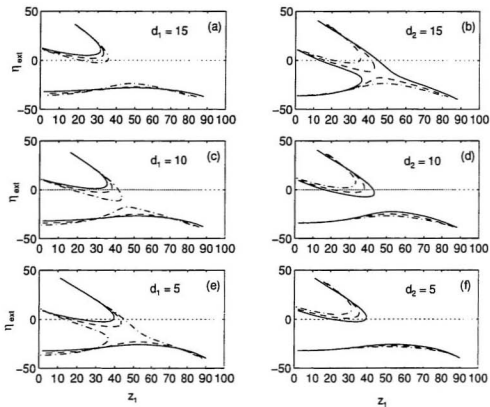


Figure 6.14: Variation of η_{ext} as a function of z_1 for density 2 with $a_1 = a_2 = 0.01$ and $z_2 = 80$ without the Boussinesq approximation. Panel (a), (c), (e): d_1 fixed and $d_2 = 5$ (solid line), 10 (dashed line) and 15 (dash dotted line); panels (b), (d), (f): d_2 fixed and $d_1 = 5$ (solid line), 10 (dashed line) and 15 (dash dotted line).

a flat-centred internal solitary wave. Figure 6.15 shows the three solutions for two-pycnocline stratification with $z_1 = 30$ and $z_2 = 80$ using $d = 10$ (see Figure 6.5). The extreme isopycnal displacements corresponding to the three solutions are -30.37, -3.08, 19.31. Internal solitary waves corresponding to the large depression and the elevation solutions are easily simulated using the fully nonlinear model described in Chapter 3. (Figures 6.16 and 6.17). Waves corresponding to the small depression have not been found. Whether they exist or not is not known. More energy is needed to obtain the flat-centred waves of depression than the flat-centred waves of elevation. This is because the centre of one pycnocline is displaced to a position near the mid-depth and the distance of the upper pycnocline to the mid-depth is larger than the lower pycnocline. Hence, when the two pycnoclines are not symmetric about the mid-depth, the two kinds of internal solitary waves, one elevated and the other depressed, can still be obtained, although the magnitude of the extreme isopycnal displacements and propagation speeds of the two waves are no longer the same. Solitary waves corresponding to the two conjugate flow solutions for the case $z_1 = 10$, $z_2 = 60$ with $d = 10$ were also sought (see Figure 6.5). Flat-centred internal solitary wave depressions were easily obtained (see Figure 6.18) with the same propagation speed and maximum isopycnal displacement given by the conjugate flow depression. Waves corresponding to the conjugate flow elevation were not obtained. This indicates that for the two-pycnocline case not all conjugate flow solutions necessarily correspond to flat-centred internal solitary waves.

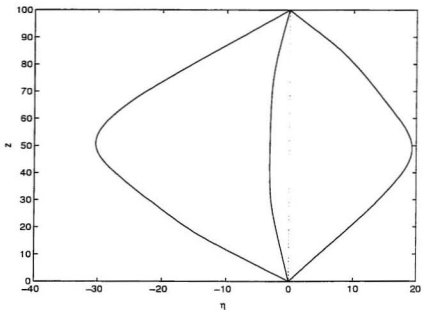


Figure 6.15: $\eta(z)$ profiles showing the three conjugate flow solutions for density 2 with $a_1 = a_2 = 0.01$, $d_1 = d_2 = 10$, $z_1 = 30$, $z_2 = 80$.

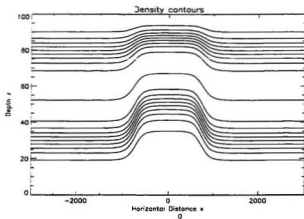


Figure 6.16: Solitary wave corresponding to the elevation solution in Figure 6.15.

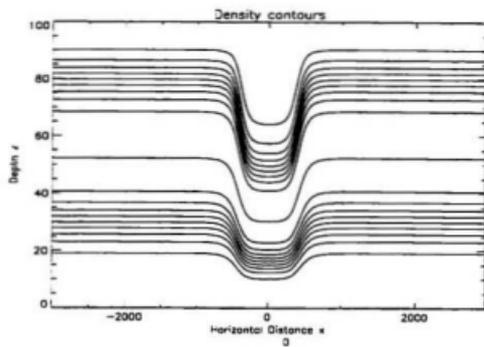


Figure 6.17: Solitary wave corresponding to the larger depression solution in Figure 6.15.

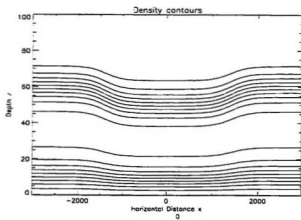


Figure 6.18: Solitary wave corresponding to the depression solution for the case $z_1 = 10$, $z_2 = 60$ using $d = 10$.

Chapter 7

Summary and Conclusion

For some stratifications internal solitary waves become flat in the centre at large amplitudes. The horizontal uniform flow in the centre of such waves is conjugate to the undisturbed flow outside of the wave. In this thesis a theoretical model which describes the flow structure in the centres of flat-centred internal solitary waves has been developed based on the conjugate flow concept. The conjugate flow solutions have been shown to give the flow in the centre of such waves, easily providing such quantities as the extreme isopycnal displacement, wave propagation speed, and the maximum fluid velocity. Flat-centred internal solitary waves can exist only if there is a conjugate flow solution. Stratifications given by hyperbolic tangent density profiles with one and two pycnoclines were considered. It was found that in order to obtain the non-zero conjugate flow solution the maximum density stratification should occur somewhere between the two boundaries; if the centre of the pycnocline is too close to

a boundary, there is no conjugate flow solution. This indicates that there should be no conjugate flow solutions if the buoyancy frequency varies monotonically from one boundary to the other. Solutions with and without the Boussinesq approximation are compared. It was found that when the density difference from surface to bottom is 4% or less, the non-Boussinesq effects are small (errors $\ll 1\%$); if the density difference is of the order of 10% or larger, the non-Boussinesq effects can be significant. The exception for this is if the pycnocline has a thickness comparable to half the fluid depth (e.g., $d >$ about 20), in which case the Boussinesq approximation can result in larger errors, or completely false predictions of the existence of conjugate flow solutions.

For the density stratification with a single pycnocline, in the conjugate flow region the pycnocline is displaced toward the mid-depth. In the Boussinesq case the centre of the pycnocline is in fact displaced slightly past the mid-depth. The magnitude of the extreme isopycnal displacement grows as the centre of the pycnocline in the undisturbed flow region moves away from the mid-depth. When the centre of the undisturbed pycnocline is too close to the surface or bottom boundary there is no valid conjugate flow solution because of $\eta'(z) > 1$ somewhere. In this case, as the wave amplitude increases the internal solitary wave grows and the breaking limit (vertical isopycnals) is reached before a flat-centred internal solitary wave is formed. When the Boussinesq approximation is applied, the wave propagation speed increases as the centre of pycnocline in the undisturbed region moves toward the mid-depth.

The analysis of conjugate flow solutions for single-pycnocline stratifications also shows that horizontal shear flow in the centre of a flat-centred internal solitary wave is linearly stable (minimum Richardson number > 0.25) if the pycnocline is sufficiently thick. In our calculations, the condition for the thickness parameter d is $d \geq 8.4$. For thinner pycnoclines the flow is potentially unstable for a range of pycnocline positions and the region of potentially unstable flow increases as d decreases. The results show that the flow is potentially unstable for all values of z_0 between 0 and H as $d \rightarrow 0$. This is identical to the result of the two-layer limit where the flow is always unstable at sufficiently small wavelength as the velocity is discontinuous across the interface.

For the stratifications with two pycnoclines, if the two pycnoclines are equidistant from the mid-depth with their centres a distance of between 17.56 and 36 from the mid-depth, two conjugate flow solutions are obtained. One is an elevation and the other is a depression of an internal solitary wave. The solutions corresponding to the elevation and depression have the same magnitudes of wave amplitude and propagation speed if the Boussinesq approximation is applied. When one pycnocline is centred in between 0 and 14, there are no valid solutions because the waves break down. When one pycnocline is centred between 32.44 and 50, there are no solutions in the Boussinesq case; but there is a small elevation in the non-Boussinesq case.

The most significant result for some density stratifications with two pycnoclines are the occurrence of three conjugate flow solutions. This occurs only when the two pycnoclines are in the upper and lower half layers of the fluid respectively and

the relative strengths of the two pycnoclines are comparable. If one pycnocline is much stronger than the other (e.g., $a_1 = 10a_2$), this phenomenon does not occur. For $a_1 = 10a_2$, the results are much like the case of a single pycnocline centred at z_1 . If the stratification variation is caused by the variation of d_1 and d_2 , the thinner pycnocline seems to have a larger effect on the results. Our investigation indicates that the stronger pycnocline (represented by a larger density gradient) seems to dominate the conjugate flow. If the difference of the strength of the two pycnoclines is very large, the results would be similar to the case where only the stronger pycnocline were presented.

The internal solitary waves corresponding to the multiple conjugate flow solutions were sought. It was found that for the stratification in which three conjugate flow solutions exist, only two internal waves corresponding to two of the three solutions were obtained: for the stratification in which two conjugate flow solutions exist and N^2 is not symmetric about the mid-depth, only one flat-centred internal solitary wave corresponding to one of the solutions was easily obtained. The physical significance of the conjugate flow solutions for which there is no corresponding flat-centred internal solitary wave is unknown.

References

- Akylas, T.R. and R.H. Grimshaw. 1992: Solitary internal waves with oscillatory tails. *J. Fluid Mech.*, 242, 279 - 298.
- Amick, C.J. and R.E.L. Turner. 1986: A global theory of internal solitary waves in two-fluid systems. *Trans. Amer. Math. Soc.*, 298, 431 - 484.
- Apel, J.R., H.M. Byrne, J.R. Proni and R.L. Charnell. 1975a: Observations of oceanic internal and surface waves from the Earth Resources Technology Satellite. *J. Geophys. Res.*, 80, 865 - 881.
- Apel, J.R., J.R. Proni, H.M. Byrne, and R.L. Sellers. 1975b: Near-simultaneous observations of intermittent internal waves on the continental shelf from ship and aircraft. *Geophys. Res. Lett.*, 2, 128 - 131.
- Apel, J.R., J.R. Holbrook, A.K. Liu and J. J. Tsai. 1985: The Sulu Sea internal soliton experiment. *J. Phys. Oceanogr.*, 15(12), 1625 - 1651.
- Benjamin, T.B., 1962a: The solitary wave on a stream with an arbitrary distribution of vorticity. *J. Fluid Mech.*, 12, 97 - 116.
- Benjamin, T.B., 1962b: Theory of the vortex breakdown phenomenon. *J. Fluid Mech.*, 14, 593 - 629.
- Benjamin, T.B. 1966: Internal waves of finite amplitude and permanent form. *J. Fluid Mech.*, 25, 241 - 270.

- Benjamin, T.B., 1967: Internal waves of permanent form in fluids of great depth. *J. Fluid Mech.*, 255, 559 - 592.
- Benney, D.J. 1966: Long nonlinear waves in fluid flows. *J. Math. Phys.*, 45, 52 - 63.
- Benney, D.J. and D.R. Ko. 1978: The propagation of long large amplitude internal waves. *Stud. Appl. Math.*, 59, 187 - 199.
- Benney, D.J. and R. Grimshaw, 1982: Large amplitude solitary waves in unbounded stratified fluids. *Stud. Appl. Math.*, 66, 181 - 187.
- Buneman, O., 1969: A compact non-iterative Poisson solver. SUIPR Rept. 24. Stanford Univ., Stanford, Calif., May 1969.
- Cummins, P.F., and P.H. Le Blond, 1984: Analysis of internal solitary waves observed in Davis Straight. *Atmos. Ocean*, 22(2), 173 - 192.
- Davis, R.E. and A. Acrivos, 1967: Solitary internal waves in deep water. *J. Fluid Mech.*, 29, 593 - 607.
- Dorr, F.W., 1970: The direct solution of the discrete Poisson equation on a rectangle. *SIAM Rev.*, 12, 248 - 263.
- Evans, W.A. and M.J. Ford, 1996: An integral equation approach to internal (2-layer) solitary waves. *Phys. Fluids*, 8(8), 2032 - 2047.

- Evans, W.A. and M.J. Ford, 1996: An exact integral equation for solitary waves (with new numerical results for some internal properties). *Proc. R. Soc. Lond. A.*, 452, 373 - 390.
- Fu, L.L. and B. Holt, 1984: Internal waves in the Gulf of California: Observation from a space-borne radar. *J. Geophys. Res.*, 89,2053 - 2060.
- Funakoshi M. and M. Oikawa, 1986: Long internal waves of large amplitude in a two-layer fluid. *J. phys. Society of Japan.*, 55(1),128 - 144.
- Gear, J.A. and R. Grimshaw, 1983: A second-order theory for solitary waves in shallow fluids. *Phys. Fluids.*, 26(1), 14 - 29.
- Grimshaw, R.H. and D.I. Pullin, 1986: Extreme interfacial waves. *Phys. Fluids.*, 29(9), 2802 - 2807.
- Halpern, D., 1971a: Observations on short period internal waves in Massachusetts Bay. *J. Mar. Res.*, 29, 116 - 132.
- Halpern, D., 1971b: Semidiurnal internal tides in Massachusetts Bay. *J. Geophys. Res.*, 76, 6573 - 6583.
- Haury, L.R., M.G. Briscoe and M.H. Orr, 1979: Tidally generated internal wave packets in Massachusetts Bay. *Nature*, 278, 312-317.
- Helfrich, K.R., W.K. Melville and J.W. Miles, 1984: On interfacial solitary waves over slowly varying topography. *J. Fluid Mech.*, 149, 305 - 317.

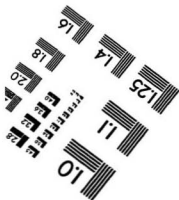
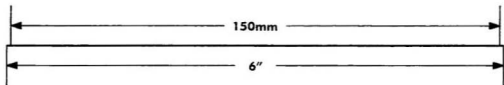
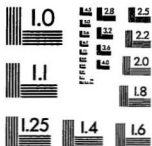
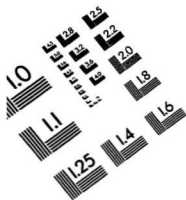
- Helfrich, K.R. and W.K. Melville, 1986: On long nonlinear internal waves over slope-shelf topography. *J. Fluid Mech.*, 167, 285 - 308.
- Helfrich, Karl R., 1992: Internal solitary wave breaking and run-up on a uniform slope. *J. Fluid Mech.*, 243, 133 - 154.
- Hockney, R.W., 1965: A fast direct solution of Poisson's equation using Fourier analysis. *J. Assoc. Comput. Mach.*, 12, 95 - 113.
- Joseph, R.I., 1977: Solitary waves in a finite depth fluid. *J. Phys. A Math. Gen.*, 10, 1225 - 1227.
- Kao, T.W., F.S. Pan, and D. Renouard, 1985: Internal solitons on the pycnocline: generation, propagation, and shoaling and breaking over a slope. *J. Fluid Mech.*, 169, 19 - 53.
- Keulegan, G.H., 1953: Characteristics of internal solitary waves. *J. Res. Natl Bur. Standards.*, 51, 133 - 140.
- Koop, C.G., and G. Butler, 1981: An investigation of internal solitary waves in a two-fluid system. *J. Fluid Mech.*, 112, 225 - 251.
- Kubota, T., D.R.S. Ko and L.D. Dobbs, 1978: Propagation of weakly nonlinear internal waves in a stratified fluid of finite depth. *J. Hydraulics.*, 12, 157 - 165.

- Kundu, P.K.. 1990: Fluid Mechanics. Academic Press, 638p.
- Lamb, K.G.. 1994: Numerical experiments of internal wave generation by strong tidal flow across a finite amplitude band edge. *J. Geophys. Res.*, 99(C1), 843 - 864.
- Lamb, K.G. and Liren Yan, 1996: The evolution of internal wave undular bores: comparisons of a fully nonlinear numerical model with weakly-nonlinear theory. *J. Physical Oceanography* (in press).
- Lamb, K.G.. 1997: Lagrangian transport by solitary internal waves. Submitted to *J. Geophys. Res.*
- Lee, C.Y. and R.C. Beardsley, 1974: The generation of long nonlinear internal waves in a weakly stratified shear flow. *J. Geophys. Res.*, 79, 453 - 462.
- Liu, A.K., J.R. Holbrook and J.R. Apel, 1985: Nonlinear internal wave evolution in the Sulu Sea. *J. Phys. Oceanogr.*, 15(12), 1613 - 1624.
- Long, R.R.. 1956: Solitary waves in one- and two-fluid systems. *Tellus*, 8, 460.
- Long, R.R., 1965: On the Boussinesq approximation and its role in the theory of internal waves. *Tellus*, 17, 46 - 52.
- Meiron, D. and P. Saffman, 1983: Overhanging interfacial gravity waves of large amplitude. *J. Fluid Mech.*, 129, 213 - 218.

- Miles, J.W., 1979: On internal solitary waves. *Tellus*, 31, 456 - 462.
- Miles, J.W., 1981: On internal solitary waves. II. *Tellus*, 33, 397 - 401.
- Ono, H., 1975: Algebraic solitary waves in stratified fluids. *J. Phys. Soc. Japan*, 39, 1082 - 1091.
- Osborne, A.R and T.L. Burch, 1980: Internal solitons in Andaman Sea. *Science*, 208, 451 - 460.
- Ostrovsky, L.A. and Y.A. Stepanyants, 1989: Do internal solitons exist in the ocean? *Reviews of Geophysics*, 27, 293 - 310.
- Pingree, R.D and G.T. Mardell, 1985: Solitary internal waves in the Celtic Sea. *Prog. Oceanogr.*, 14, 431 - 441.
- Pullin, K.I and R.H. Grimshaw, 1988: Finite-amplitude solitary waves at the interface between two homogeneous fluids. *Phys. Fluids*, 31(12), 3550 - 3559.
- Roache, P.J., 1978: Marching methods for elliptic problems: Part 1. *Numerical Heat Transfer*, 1, 1 - 25.
- Sandstrom, H. and J.A. Elliott, 1984: Internal tide and solitons on the Scotian Shelf: a nutrient pump at work. *J. Geophys. Res.*, 89, 6415 - 6426.
- Stamp, A.P. and M. Jacka, 1995: Deep-water internal solitary waves. *J. Fluid Mech.*, 305, 347 - 371.

- Turner, R.E.L. and J.M. Vander-Broeck, 1988: Broadening of interfacial solitary waves. *Phys. Fluids*, 31(9), 2486 - 2490.
- Tung, K.K., T.F. Chan and T. Kubota, 1982: Large amplitude internal waves of permanent form. *Studies in Applied Mathematics*, 66, 1 - 44.
- Turkington, B., A. Eydeland and S. Wang, 1991: A computational method for solitary internal waves in a continuously stratified fluid. *Studies in Applied Mathematics*, 85, 93 - 127.

RESOLUTION EVALUATION
TEST TARGET (QA-3)



APPLIED IMAGE, Inc
1653 East Main Street
Rochester, NY 14609 USA
Phone: 716/482-0300
Fax: 716/298-5989

© 1993, Applied image, inc., All Rights Reserved

